The Cryosphere Discuss., https://doi.org/10.5194/tc-2018-5
Manuscript under review for journal The Cryosphere
Discussion started: 20 March 2018

The Cryosphere Discussions
Open Access
EGU

A statistical fracture model for Antarctic ice shelves and glaciers

Veronika Emetc[1], Paul Tregoning[1], Mathieu Morlighem[2], Chris Borstad[3], and Malcolm Sambridge[1]

[1]Research School of Earth Science, Australian National University, Canberra, Australia
[2]Department of Earth System Science, University of California, Irvine, USA
[3]Department of Arctic Geophysics, The University Centre in Svalbard

Correspondence to: Veronika Emetc (Veronika.Emetc@anu.edu.au)

Abstract. Antarctica and Greenland hold enough ice to raise sea level by more than 65 m if they were to melt completely. Predicting future ice sheet mass balance depends on our ability to model these ice sheets, which is limited by our current understanding of several key physical processes, such as iceberg calving. Large scale ice flow models either ignore this process or represent it crudely. To model fracture formation, which is an important component of many calving models, Continuum Damage Mechanics as well as Linear Fracture Mechanics are commonly used. However, these methods applied across the Antarctic continent have a large number of uncertainties. Here we present an alternative, statistics-based method to model the most probable zones of nucleation of fractures. We test this approach on all main ice shelf regions in Antarctica, including the Antarctic Peninsula. We can model up to 99% of observed fractures, with an average rate of 84% for grounded ice and 61% for floating ice and mean overestimation error of 26% and 20%, respectively, thus providing the basis for modelling calving of ice shelves. We find that Antarctic ice shelves can be classified into groups based on the factors that control fracture location. The factors that trigger fracturing as well as sustain existing fractures advected from upstream vary from one ice shelf to another.

Keywords. Antarctic, ice shelves, glaciers, probability, calving, fracture nucleation, crevasse, logistic regression, bayesian

1 Introduction

In recent years, increased positive temperature anomalies have been observed in Antarctica (Jansen et al., 2007; Vaughan et al., 2003; Johanson and Fu, 2007; Steig et al., 2009) and future climate change in this area may be even more pronounced (Vaughan et al., 2003). This may cause the state of the Antarctic Ice Sheet to change significantly and could lead to a release of fresh water currently stored in the ice sheet; West Antarctica alone could contribute up to 4.3 metres to global sea level (Fretwell et al., 2013). Thus, understanding the factors that control the mass balance of the Antarctic ice sheet is crucial if we want to better understand the future impact of climate change and contribution of Antarctic ice mass loss to global sea level rise (SLR).

Ice sheet mass loss is controlled by three processes: surface ablation, basal melting and calving, where the latter also controls the amount of buttressing that floating ice shelves exert onto the ice streams feeding them. Due to the fact that the surface ablation in Antarctica is relatively low, it was previously believed that the Antarctic ice sheet was stable. However, increased calving from the major ice shelves between 1998 and 2003 led to a growing concern about the ice sheet stability (Shepherd et al., 2012).

The Cryosphere Discuss., https://doi.org/10.5194/tc-2018-5
Manuscript under review for journal The Cryosphere
Discussion started: 20 March 2018

Overall, research on crevasse propagation started as early as 1955 and calving parameterization has been under development for the last 20 years. It has been shown that the increased ice mass loss from Antarctica is caused primarily by an increased number of calving events in the last two decades which led to significant ice front retreat (e.g., the collapse of Larsen B ice shelf and potential break off a part of Larsen C ice shelf (Mercer, 1978; Jacobs et al., 1992; Katz and Worster, 2010; Gudmundsson, 2013; Borstad et al., 2013)). Studies by Jezek (1984); De Angelis and Skvarca (2003); Dupont and Alley (2005); Goldberg et al. (2009); Katz and Worster (2010); Gudmundsson (2013); Borstad et al. (2013) showed that increased calving can lead to destabilization of ice shelves and thus to a loss of the supporting mechanism they provide to inland ice in Antarctica. This support can be crucial for the overall stability of the West Antarctic ice sheet (Miles et al., 2013) as it can be potentially unstable in case of strong basal melting and reduced ice shelf buttressing.

In order to develop a reliable calving law, it is essential to know where these fractures are located and how they evolve. There have been a number of approaches that successfully modelled rift formation on particular ice shelves, but this is still an active area of research, and none of the current studies have been looking at the scale of Antarctica and a method that can universally describe calving at any ice shelf in Antarctica has not been found yet.

In this study, we focus on modelling of crevasses (surface fractures less than 200 metres wide) on the surface of the Antarctic ice sheet. Our model to predict zones of fracture formation is based on a probabilistic approach, where we utilize the logistic regression algorithm (LRA) to find a relationship that enables the prediction of fracture initiation. We applied this approach to most of the Antarctic ice shelves as well as grounded ice regions around ice shelves in both West and East Antarctica and to the Antarctic Peninsula. Our approach is comprehensive in the sense that it accounts for many potential parameters that include geometry, mechanical properties and flow regime. Moreover, it is based on a combination of remote sensing and modeling. The dataset of fracture observations is built by carefully manually selecting the locations of visible fractures in satellite images, after which it is corrected using a damage-based model suggested by Borstad et al. (2013). Using this observations and predictor parameters we were able to build a model that can describe fracture formation for many ice shelves in Antarctica. From modelling of 45 ice shelves/glaciers, we found that we can predict fracture locations that match the observations of fractures with a success rate from just below 45% to 99% with an average success rate of 84% (Figure 1a) for grounded ice and 61% for floating ice (Figure 1b) and a mean overestimation error of 26% and 20%(we found that the average success rate when applying damage method to floating ice to be equal to 34%). Our best results were achieved combining LRA with Bayesian as well as Jensen-Shannon Divergence theory described in section 3.

with a mean overestimation error of 26% and 20%

2 Background

2.1 Current state of calving computations in ice sheet models

A number of calving parameterisations have been developed and implemented in some software packages, but none of them includes the propagation of fractures in both depth and horizontal space. Most of the available parameterisations are specific to a particular case and set of predictors, or a location, and therefore cannot be applied generically to any ice shelf.

The Cryosphere Discuss., https://doi.org/10.5194/tc-2018-5
Manuscript under review for journal The Cryosphere
Discussion started: 20 March 2018

Some ice sheet models, such as ELMER/Ice, the Parallel Ice Sheet Model (PISM), the Community Ice Sheet Model (CISM) as well as the Ice Sheet System Model (ISSM), have attempted to include calving built on simplified physics (Alley et al., 2008): ISSM has a calving algorithm for marine terminating glaciers derived from a tensile Von Mises yield criterion (Morlighem et al., 2016). PISM uses a calving algorithm based on along and across-flow strain rate (Levermann et al., 2012), which is based on the correlation between the calving rate and the first order approximation of local ice-flow spreading rate (it includes spreading rates of the first-order and assigns all higher order terms to zero). The idea is based on the observations of the increase of calving rate with along-flow ice shelf spreading rates and the spreading rates perpendicular to the calving front. However, it considers only large-scale behaviour and does not take into account the formation and propagation of crevasses. The second method implemented in PISM involves calculating a calving rate based on the critical ice thickness, which is mainly used to model calving of marine-terminating glaciers rather than floating ice shelves (due to different physics governing calving between the grounded ice and floating ice). Most of the experiments with ELMER/Ice calving were performed for Greenland glaciers, which have a different calving mechanism from the floating ice shelves in Antarctica (Van der Veen, 2002). The Community Ice Sheet Model (CISM) assumes that calving takes place when the water depth reaches a certain value (Price et al., 2014). This water-depth calving model uses flotation criteria to estimate the location of the glacier terminus. It allows calving to be linked to glacier dynamics as well as surface melting when applied to marine-terminating glaciers in Greenland (Nick et al., 2010). However, it cannot describe calving at floating ice shelves in Antarctica since there floating part is simply removed from the model (the water-depth relationship requires a glacier to calve once it floats).

A number of other approaches have advanced our understanding of calving and the main studies are presented in Table 1. We can see that, to date, Continuum Damage Mechanics (Kachanov, 1958) and Linear Elastic Fracture Mechanics (Van der Veen, 1998a) are the most common methods used to model fracture formation, which is an important process that needs to be accounted for when modelling calving. The LEFM approach by Krug et al. (2014) consists of calculating a stress intensity factor around fractures and assuming that they propagate until the factor falls below a certain critical value. To apply this method to any ice shelf, the modelled fractured zones need to be in good agreement with the observed surface fractures. Therefore, modelling the formation of the fractured zones is an important basis for the subsequent estimation of fracture depth as well as calving and it needs to be described in the ice sheet models in an accurate way. On the other hand, the method proposed by Borstad et al. (2016) can describe both formation and potential evolution of fractures, however since this approach describes only viscous behaviour it is still to be coupled with an elastic damage model (Borstad et al., 2016).

In addition, Krug et al. (2014) built an alternative scheme by combining LEFM and CDM and found that they could match evolution of a tidewater glacier. This method is more complex in comparison to the other approaches suggested before 2014 as it allows for both viscous and elastic behaviour and is able to reproduce development of small crevasses over a long period of time. The ELMER/Ice model (Gagliardini et al., 2013) includes calving combining CDM and LEFM, but this method has only been applied to Greenland (Krug et al., 2014) and has not yet been applied to ice shelves in Antarctica. There are a number of other studies that proposed other calving laws (Pralong and Funk, 2005; Duddu and Waisman, 2012), but they might be not applicable in a generalised large-scale case.

Fracturing of Antarctic ice shelves can be seen in satellite imagery, with fractures occurring as often as every 50 m. Making in situ observations of such fracture patterns in Antarctica is not feasible due to the very large regional extent of ice shelves. Satellite observations provide the only means of making such observations but can be incomplete because of the very high resolution required to see all the fractures, and snow can often cover the fractures in images. It is for these reasons that inverse methods are often used (Borstad et al., 2013, 2016). because of the incomplete knowledge of fracturing in Antarctica, the main factors that lead to fracturing in ice shelves/glaciers remain unclear.

2.2 Continuum Damage Mechanics approach in ice sheet models

We utilise a damage-based model in order to compare it with the observations of fractures and to identify areas where it can and cannot accurately predict the observations. We do not compare our probability-based model with the damage model directly; rather, we evaluate their respective ability to predict the formation of fractures in ice. It is important to note that physics-based methods, such as Linear Elastic Fracture Mechanics (LEFM) and Continuum Damage Mechanics (CDM), are necessary when modelling fractures in Antarctica. We do not intend to substitute them; rather, we seek a method that can improve on some aspects and cases when physics-based models do not predict well the formation of fractures. In addition, we use the damage model to correct the observation of fractures in order to distinguish initiated fractures from fractures that are advected from upstream.

The Continuum Damage Mechanics approach, based on the method suggested by Kachanov (1958), includes estimation of damaged zones where the ice is softened due to the presence of fractures. Damage is a scalar variable used to determine failure of ice and nucleation of fractures, usually when the damage predictor reaches a certain value. Continuum Damage Mechanics has been successfully applied to a wide range of engineering problems as well as to model damage at individually selected ice shelves such as the Ross, Filchner-Ronne, Amery (Bassis and Ma, 2015), Larsen C (Borstad et al., 2013) and Larsen B (Borstad et al., 2016) ice shelves.

It is important to distinguish between methods applied to invert for damage and methods used to model damage propagation in ice sheet models. There are two different methods for inverting for damage. Borstad et al. (2012) suggested a direct inversion for damage using a cost function. Later, Borstad et al. (2013) proposed a method to calculate damage as a post-processing routine after inverting for the ice viscosity. First, inversion of ice rheology is performed following Larour et al. (2005), then damage is calculated from the inversion of velocities at the ice shelves, which is based on minimising the cost function that quantifies the misfit between the observed and modelled surface velocities.

The second stage includes propagation of damage. (Krug et al., 2014; Albrecht and Levermann, 2014) proposed modelling the propagation of damage using an advection scheme and a source function. The main limitations of this method are the choice of what should be used as a source function as well as the number of decisive parameters that define the damage evolution (damage threshold, initiation threshold and the enhancement factor). The source function is the controlling factor in the damage propagation and Pralong et al. (2003) as well as Krug et al. (2014) proposed a source function definition. Both of the approaches work well for a particular region, but control predictors in this model have been calculated for only one specific glacier in Greenland (Duddu and Waisman, 2012) and through using small-scale laboratory experiments (Pralong and Funk,

2005) and have not yet been generalised to be applicable to all ice shelves/glaciers. This models also have not yet accounted for factors such as ice fabric and impurities (Borstad et al., 2012).

Recently, Borstad et al. (2016) proposed a framework where, instead of computing a damage source term as is usually done, damage is part of a generalized constitutive relationship. This approach has a number of advantages as it allows the calculation of mechanical ice weakening and predicting degradation of ice shelves. This can significantly improve the accuracy of identifying the zones where the ice is weakened by illuminating the uncertainties related to the source function. The main difficulty comes from determining the constant parameters that define damage, because the validity of the parameter values can only be tested when an ice shelf undergoes pronounced mechanical changes, as did the Larsen B Ice Shelf in 2002. The parameters suggested by Borstad et al. (2016) have not been tested for other ice shelves apart from Larsen B, and so it is unknown whether the approach is valid for other locations and settings.

In this study we use the damage inversion method proposed by Borstad et al. (2013) to identify regions where fractures are initiated. This approach is performed in two steps. First, the inversion of rheology based on the misfit between observed and modelled velocity is performed on floating ice. Then, damage is calculated using equation:

$$D = 1 - \frac{B_I}{B_T}, \tag{1}$$

where B_I and B_T are viscosity parameters calculated from an inversion and initialisation of viscosity based on temperature analysis, respectively.

Estimation of B_T is the source of the main uncertainty in damage calculations due to the lack of ice temperature data, which can be crucial in affecting the accuracy of the viscosity parameter (Bassis and Ma, 2015). Damage is calculated only on floating ice based on model inversions using the Ice Sheet System Model (ISSM) (Larour et al., 2012) because it is not possible to distinguish between basal friction and damage on grounded ice, as they have similar effects on the ice velocity.

It is possible that some fractures are initiated upstream of the grounding line rather than on floating ice. It is therefore important to be able to predict the formation of fractures in both cases. Thus, the main motivation of this study is not to replace the damage approach, which in fact provides a strong physical background for ice sheet modelling, but to find an alternative method that can be applied to both ice shelves and grounded ice, can work for a large set of glaciers/ice shelves and does not depend on temperature observations and threshold parameters. As described in Section 3.1, our model uses as input ice sheet geometry and dynamics parameters in a 450-metre resolution, and we parameterise the model to depend upon observed location of fractures.

2.3 Ice Sheet System Model (ISSM) Model setup

To derive quasi-observations for our statistical model, we use ISSM (Larour et al., 2012) to compute velocities, stresses, strains, backstresses as well as friction coefficient and viscosity (calculated from inverse modelling). All our experiments were performed for 46 ice shelf regions in Antarctica (see Figure 2a), each including both ice shelves and the grounded ice around 100 kilometres upstream from the grounding line (hereafter referred to as ice shelf regions or ice shelf/glacier).

ISSM is a fully dynamic model that includes both 2 dimensional (2-D) and 3-D stress balance approximations and e rely here on the shelfy stream approximation (SSA), as it is computationally cheap and suitable for modelling floating ice shelves.

To perform a simulation, we used SeaRISE air temperature, snow accumulation and geothermal heat flux (Le Brocq et al., 2010) as climate forcing data. We calculated changes of the surface temperature with a lapse rate and imposed it on the ice surface. The data for the geometry of the ice shelves and surrounded grounded ice (bedrock topography, ice thickness and glacier surface) were interpolated from Bedmap2 data at 1 km spatial resolution. We used these data as input for our modelling using ISSM and as the predictor factors in our probabilistic method (see Section 3.1). The position of the grounding line position is calculated using a flotation criterion.

Basal friction under grounded ice and rheology for floating ice were calculated from an inversion of velocities (Khazendar et al., 2007). The initial friction coefficient was set equal to 10. In the inversions we used regularisation to penalise sharp gradients of the cost function, calibrated using an L-curve analysis (Morlighem et al., 2013). The horizontal ice velocities for the inverse modelling were taken from InSAR (450-metres resolution) (Rignot et al., 2011b, a) and we applied Dirichlet conditions at the inflow boundary.

We set boundary conditions as follows: the upper surface is considered stress-free and friction is applied at the ice-bedrock interface. We ran one simulation to create a stress balance solution per region (ice shelf/glacier), which allowed us to obtain the factors required as input in the calculation of the probability of fracturing.

It is important to have a fine resolution mesh in order to model surface fractures, as the distance between them is normally around 50-100 metres. However, using a 50- or 100-metre mesh resolution created a significant increase in the computational time of the model. Therefore, for our experiments, we used a multi-resolution mesh approach for the chosen domains in East and West Antarctica as well as the Antarctic Peninsula. We first calculated all the main predictors on a 200-metre resolution mesh (to achieve a faster computational speed) and then interpolated the values to a 100-metre resolution mesh (to use in our fracture model resolved at 100-metres). All further computations and analysis were performed on this finer mesh.

3 Methods

To develop an alternative method for modelling fracture formation in ice shelves/glaciers, we took into account that the damage varies from 0 to 1 in a probabilistic sense, with 0 being not fractured and 1 being fully fractured. We can substitute this probability with a likelihood function and can then apply this method to to derive fracture likelihood functions for both floating ice shelves and the grounded ice. It is important to note that where fractures are formed is not necessary where they are visible in satellite imagery. Fractures can be located in a certain place as a result of advection of fractures from upstream (high-advection) or because of local stresses (low advection) (Colgan et al., 2016). We do not distinguish between these high-advection and low-advection cycles in our approach. Our main goal is to determine the most likely location of fractures without focusing on their initial source. Thus, to implement our ice calving model into the ice sheet models, we developed a statistical-based parameterization for fracture formation in ice shelves/glaciers.

The Cryosphere Discuss., https://doi.org/10.5194/tc-2018-5
Manuscript under review for journal The Cryosphere
Discussion started: 20 March 2018

Even if a fracture did not form at a particular location, but is advected with the ice flow, it is possible that a certain combination of factors could close the fracture, which would then not be visible on the satellite image. The fact that fractures can be seen indicates that there are certain other factors that act to permit the fractures to exist, whether they formed in that particular location or remained open after being advected there from upstream. Using this approach, we do not directly model advection, but predict the locations of both initiated and advected fractures. First, we present our method (logistic regression) used for predicting the formation of fractures. Second, we describe the predictor factors (predictors) we used in our analysis. Finally, two methods used for optimising a set of predictor factors are presented (Bayesian based algorithm and Jensen-Shannon Divergence).

3.1 The logistic regression algorithm (LRA)

Let the function P be a logistic function. Taking any range of data it produces values from 0 to 1 and thus it can be used as a probability (Hosmer Jr and Lemeshow, 2004). The logistic function allows us to calculate the probability of an event as a function of different predictor factors (see Table 2).

We started with a set of 21 predictors, x_i. Some of them are known to influence fracture formation (stresses, strains, changes of the velocity gradient, ice rheology). Others we considered to be potentially important (various geometrical properties, proximity to the ice front and the grounding line, etc). Temperature and accumulation were excluded from the list of predictors due to the incompatibility of their spatial resolution with the relatively fine 100-metre mesh we used to model fractures. They might be important for the formation and propagation of fractures, as warmer temperatures can increase the number of fractures, but a better resolution climate dataset would be needed to assess this. Excluding these two factors, we obtained a set of 19 predictors that we describe below.

The data for building the statistical model are taken from 35 glaciers, we used another 10 glaciers (36 to 45) to test how well our new approach predicts fractures from randomly chosen ice shelf regions that are not a part of the data used to build the model.

To apply the logistic regression algorithm we constructed a function P (Eq. 2) that describes the probability of fracture in a certain node as a function of the predictor factors x_i. It is important to note that this function does not provide any information about the depth of a fracture, just its spatial location.

Eachelement j in the P array can be calculated as:

$$P_j = Prob(X = 1|x_i) = \frac{\exp(\beta_0 + \beta_1 \cdot x_{1j} + \beta_2 \cdot x_{2j} + \beta_3 \cdot x_{3j} + ...)}{1 + \exp(\beta_0 + \beta_1 \cdot x_{1j} + \beta_2 \cdot x_{2j} + \beta_3 \cdot x_{3j} + ...)}, \quad (2)$$

where for x_{ij} is an element in a predictor array (i is the number of the predictor and j is a row number).
The unknown coefficients β_i can be found by maximising the likelihood function L (Eq. 3).

$$L(\beta_j) = \prod_{j=1}^{n} P_j^{\delta_j} (1 - P_j)^{1-\delta_j}, \quad (3)$$

The Cryosphere Discuss., https://doi.org/10.5194/tc-2018-5
Manuscript under review for journal The Cryosphere
Discussion started: 20 March 2018

where n is the number of observations and δ is the Kronecker symbol:

$$\delta = \begin{cases} 1, & \text{when there is a surface fracture visible on a satellite image} \\ 0, & \text{otherwise.} \end{cases} \tag{4}$$

Many parameters that are used for prediction of fractures on grounded ice are not applicable for predicting fractures on floating ice and vice versa (for example, friction and bed slope are irrelevant on floating ice, whereas backstress cannot be applied to grounded ice). Therefore, all the experiments and sets of parameters used in LRA are constructed separately for floating and grounded ice.

The calculation of some predictors was performed using methods already implemented in ISSM (e.g. stresses, strains, friction coefficient). Some predictors (e.g. calculation of curvature, distances to ice front, grounding line, proximity to glacier edges and nunataks) were calculated independently of ISSM, using new algorithms. Here we describe the methods we used to calculate each predictor parameter as well the description of why each parameter is expected to have an impact on crack propagation.

First, principal stress λ is important because it has a direct effect on the opening and closing of crevasses; the sign of the first principal stress determines whether it is compressive (negative) or tensile (positive).

$$\sigma \cdot \mathbf{s} = \lambda \mathbf{s} \tag{5}$$

Second, the effective strain rate $\dot{\epsilon}_E$ is included in our analysis because it is known that crevasse initiation is linked to strain rates (Campbell et al., 2013). If the strain rate in the horizontal plane is sufficiently high, crevasses can propagate to greater depth (Benn and Evans, 2010). In addition, stresses can trigger brittle fracturing, but to model a gradual viscous process strains have to be taken into account.

We calculated this predictor in ISSM as:

$$\dot{\epsilon}_E = \sqrt{\frac{\dot{\epsilon}_{xx}^2 + \dot{\epsilon}_{yy}^2}{2} + \dot{\epsilon}_{xy}^2}, \tag{6}$$

where $\dot{\epsilon}_{ik} = \frac{1}{2}(\frac{\partial v_i}{\partial x_k} + \frac{\partial v_k}{\partial x_i})$ and v_i are horizontal components of the ice flow velocities (InSAR).

The principal strains are calculated as:

$$\mu = \frac{\epsilon_{xx} + \epsilon_{yy}}{2} \pm \sqrt{\left(\frac{\epsilon_{xx} - \epsilon_{yy}}{2}\right)^2 + \epsilon_{xy}^2}, \tag{7}$$

The Cryosphere Discuss., https://doi.org/10.5194/tc-2018-5
Manuscript under review for journal The Cryosphere
Discussion started: 20 March 2018

Third, fractures can be formed in zones where strain experiences significant variations. Thus, the horizontal strain gradient is included as a predictor parameter.

Fourth, because back stress provides an additional compressive stress resisting the forward motion of glacier ice (Kenneally and Hughes, 2004) it is also included in our model.

Furthermore, low friction will lead to a higher sensitivity to membrane stresses, which can lead to more crevassing in tensile mode. We obtain this parameter from the inversion of velocities in ISSM.

In addition, we include the stiffness of ice as well as thickness due to their physical relation to fracture mechanics where $\boldsymbol{v}(P)$ is the ice velocity at the point of observations and $\boldsymbol{v}(E)$ is the velocity D metres away from the point. The distance D is based on the velocity magnitude $\boldsymbol{v}(P)$, because if the velocity is high we need to increase D so that two subsequent points capture the geometry of the bend of a glacier. Thus, if $\boldsymbol{v}(P)$ is greater than 2000 m/yr we assign $D = 3\boldsymbol{v}(P)$, otherwise $D = 6\boldsymbol{v}(P)$. These values are not arbitrary: this assignment is used in the model only to have enough data points to see the local curvature of a glacier and it does not affect the calculation of the curvature itself.

Generally the lateral friction along the glacier boundary is not considered in ice sheet models when stress is calculated. However, the prediction of marginal crevasses requires a parameterisation of the lateral drag. Therefore the stress field alone does not necessarily have the full ability to predict zones of fracture formation, because without the inclusion of the lateral drag only transverse, longitudinal and radial splaying crevasses can be predicted. They are all formed due to opening stress and are normally considered in existing damage modelling methods. Thus, we include the proximity to edges of glaciers and to nunataks to our model.

We can see in the satellite images that more fractures occur at a certain distance from the ice front as well as near the grounding line. We found that the relation between the occurrence of fractures and distance to the ice front as well as the distance to the grounding line is non-linear (Fig. 2b). For most ice shelves/glaciers we can see more fractures 3-5 km as well as 10-13 km away from the front and a slightly smaller number of fractures closer than 3 km to the front or between 5 and 10 km. Therefore, instead of using $\mathbf{d_{IF}}$ and $\mathbf{d_{GL}}$ (distance to the ice front and the grounding line in km) as predictor variables, we construct dummy variables: $\mathbf{DM_{IF}}$ and $\mathbf{DM_{GL}}$, respectively, which represent two-column arrays in the following form:

$$\mathbf{DM_{IF}} = \begin{cases} (1,1), & \text{when } 3\text{km} \leq \mathbf{d_{IF}} < \mathbf{5}\text{km} \\ & \text{or} \quad 10\text{km} \leq \mathbf{d_{IF}} < \mathbf{13}\text{km} \\ (1,0), & \text{when } 5\text{km} \leq \mathbf{d_{IF}} < \mathbf{10}\text{km} \\ (0,1), & \text{when } \mathbf{d_{IF}} < \mathbf{3}\text{km} \\ (0,0), & \text{else} \end{cases} \tag{8}$$

The Cryosphere Discuss., https://doi.org/10.5194/tc-2018-5
Manuscript under review for journal The Cryosphere
Discussion started: 20 March 2018

$$\mathbf{DM_{GL}} = \begin{cases} (1,1), & \text{when } 5\text{km} \leq \mathbf{d_{GL}} < \mathbf{15}\text{km} \\ (1,0), & \text{when } \mathbf{d_{GL}} < \mathbf{5}\text{km} \\ (0,1), & \text{when } 15\text{km} \leq \mathbf{d_{GL}} < \mathbf{20}\text{km} \\ (0,0), & \text{else} \end{cases} \tag{9}$$

There are a number of parameters such as velocity, surface slope and a curvature of a glacier channel that are included in the calculation of the stress field, but for our method we look at each component separately:

Thus, bed and surface slopes are included in the model since on a steeper slope, shear stress increases and can lead to fracturing (e.g. ice fall is an extreme case).

Surface gradient change: if there is a sudden change in a surface elevation the stress can increase, causing fracturing.

Curvature: it is clearly visible in satellite images that more fractures occur around horizontal bends in glaciers. Therefore, the curvature of the glacier channel was included as a predictor, calculated as:

$$\alpha = \arccos\left(\frac{v_x(P)\cdot v_x(E) + v_y(P)\cdot v_y(E)}{|\boldsymbol{v}(P)|\cdot|\boldsymbol{v}(E)|}\right), \tag{10}$$

Finally, since all predictor parameters have different units, as well as significantly different magnitudes, we normalise them, using:

$$x_i^* = \frac{x_i - \mu_i}{\sigma_i}, \text{ where } \mu_i \text{ and } \sigma_i \text{ are mean and standard deviation of the predictor variables, respectively.} \tag{11}$$

3.2 Observing fractures using satellite images

In order to obtain information about the location of fractures on the ice sheet surface we used satellite images taken from Google Earth-Pro, where images of the Antarctic ice sheet were available at different spatial resolutions. However, to be able to see small surface fractures we limited our choice to only images with a horizontal resolution smaller than 10 metres for the period between 2011 and 2015. In addition, we included only regions with good satellite coverage (at least one high resolution satellite image) and where it is relatively easy to identify surface fractures.

Many features can be observed on the ice surface and it is important to distinguish the surface fractures from other patterns such as surface troughs due to bottom crevasses or subglacial channels. It was suggested by Luckman et al. (2012) that features on the images that are wider and have a larger spacing between them are more likely to be troughs linked to bottom crevasses. In fact, Alley et al. (2016) proposed a way to distinguish basal channels and fractures on the satellite images. They classified channels into sub-glacially sourced, ocean-sourced and grounding-line-sourced. Most of them follow the ice flow direction

and begin either at the grounding-line or downstream. Therefore, we avoided including such features when identifying surface fractures. We do not mark these troughs in the figures presented in this manuscript, which could be incorrectly interpreted as fractures that our models failed to predict.

Building correct predictions for fracturing P_i requires the use of satellite images of different regions in Antarctica, as the diversity in sampling provides a better estimation of the β coefficients (the number of observation points is less important). Thus, by choosing multiple glaciers we can more accurately construct an approximate surface that separates fractured from non-fractured nodes (the plane is determined by β coefficients).

To construct the set of observed fractures we manually selected fractured points as well as non-fractured points identified in the satellite images. Non-fractured points are more difficult to identify, therefore we mainly take them from areas where high-resolution images are available. Most of the identified non-fractured regions are located in blue ice regions, being areas with low snow accumulation or where the snow has been removed by the wind. In such areas we can clearly see where the ice is not damaged. We construct a field of fractures by assigning a value of 1 to fracture nodes and 0 to non-fractured nodes. We assign nodes to be fractured only where we can see surface fractures that do not have features caused by present basal fractures or channels.

The resolution is not sufficiently high in all areas to clearly see every fracture, and some of them may be covered in snow. This creates a large uncertainty in cells where we are not able to observe any visible fractures. Sometimes it is not possible to say whether there are no fractures or whether they are just not visible. Thus, we adjusted our fracture field by using the probability of observed fractures instead of the observations of fractures in order to make the observation field continuous as well as to account for the uncertainties in our ability to observe accurately whether or not areas are fractured. In a node where we could see a fracture we assigned the observed probability to 1. We then assumed that if there is a fracture in one node then the neighbour nodes are more likely to be fractured as well. Within a radius of 500 metres away from the fracture we decreased the probability linearly from 1 to 0.55. If a non-fractured node was found within a region with high resolution imagery, we assigned the probability of fracturing in this node to 0.05. Within a 500 metres radius of non-fractured nodes we allowed the probability to increase linearly from 0.05 to 0.4. In all other nodes we set a value of 0.5, assuming that, since the information in the satellite image is ambiguous, there is an equal probability of the node being fractured or unfractured. We scaled the probability field due to the fact that the statistical approach based on logistic regression requires scaling, as in general there are more non-fractured nodes than fractured. In addition, scaling is required for the calculation of prior when applying Bayesian inversion (it produces too large values when calculating it without the scaling due to the fact that there are a large number of non-fractured nodes (if the probability of fracturing is less than 50%)).

We did not need to select all the fractures on the ice sheet surface to build the statistical model but, in order to compare the results of our model with observations, we constructed extra data sets where we made a concerted effort to select all the visible fractures on the ice surface. It is possible that some fractures were missed due to the large spatial extent of the experiments. However we do not present every fracture on the figures in this paper in order to make the figures legible.

The Cryosphere Discuss., https://doi.org/10.5194/tc-2018-5
Manuscript under review for journal The Cryosphere
Discussion started: 20 March 2018

3.3 Optimisation problem

3.3.1 Random walk

We implement our method using a 100-metre resolution models for 45 ice shelf regions in Antarctica (including floating ice and surrounded grounded ice). We started with a first guess (calculated using LRA and a random choice of the predictor parameters) and then improved it based on three methods: random walk, Bayesian and Jensen-Shannon Divergence algorithm. To construct the probability function for each glacier we needed to identify a set of the predictor factors required to include in the LRA. For each glacier, we performed a 100000-step run with random sets of predictors used at each step (that is, the number of predictors and the selection of predictors are chosen at random every step). We defined a good model to be the one with a success of identifying fractures more than 70% and the error of overestimation smaller than 15% (however, if a good-fit model was not found after 2000 steps we looked for a model with a 65% success and 20% error). Once a good fit was found, we saved it and continued running the model with different sets of predictor factors for the remaining number of steps to see if a better model could be found. This also provided a mean set of factors needed for a good-fit model.

3.3.2 Bayesian

To test the behaviour of the models with more precision and to choose an optimal set of factors from the full set we also performed a non-linear Bayesian inversion. This process has the advantage of allowing us to take into account uncertainties in the observed data.

We assumed that the prior probability density function (PDF) is uniformly distributed between 1 and 20 (U[1,20], because the maximum number of predictor factors in a set is equal to 20). As a prior model we took a calculated fracture probability at every time step. Each step included two criteria: if a new likelihood is greater than the prior likelihood or it is greater than a certain percentage (taken at random at each step) of the old likelihood we accept the model. Finding an expression for a likelihood function for our model was problematic. We tested a number of different commonly used expressions, such as:

$$\begin{cases} L_i &= \sum \log(f_i) \\ f_i &= (1-p_i)^{1-d_i} + p_i^{d_i}, \end{cases} \tag{12}$$

$$\begin{cases} L_i &= \sum \log(f_i) \\ f_i &= (1-p_i)\cdot(1-d_i) + p_i \cdot d_i, \end{cases} \tag{13}$$

where d_i and p_i are observed and modelled fractures on a glacier, respectively.

However, all of them produced very large likelihoods that increased dramatically with a small percentage change in probability density function, reaching an order of 10^5. This was unrealistic and made the inversions unstable. Thus, it was important

to choose a representative likelihood function. We constructed a likelihood function assuming that the measure R of the total agreement between two models (the sum of all probabilities) follows a Gaussian distribution with a mean E (Eq. 14) and a standard deviation as a square root of variance σ described in Equation 17.

We calculated the expected values for both the data and a chosen model as:

$$E(f_i^{pred}) = \sum_{i=1}^{N} f_i \tag{14}$$

$$E(f_i^{obs}) = \sum_{i=1}^{N} d_i^2 + (1 - d_i)^2 \tag{15}$$

$$E(f_i^{best}) = \sum_{i=1}^{N} p^* \cdot d_i + (1 - p^*) \cdot (1 - d_i), \tag{16}$$

where p^* is the best-fit probability and the probability f_i that two predictions agree in a cell i is calculated using Equation 13.

We calculated the variance as the difference between the two expected values (Eq. 17).

$$\sigma = |E(f_i^{obs}) - E(f_i^{best})| \tag{17}$$

Our idea was to calculate the likelihood L_i as an exponential function of the misfit between the data and the model, assuming that either the data (observed fractures) or the analysed model contain an error (Eq. 18). A misfit $\phi_d(m)$ can be calculated as the square of the ratio between the expectation for the data minus the expectation for the model and the variance of the data:

$$L_i = e^{-\frac{1}{2}\phi_d(m)}, \text{ where } \phi_d(m) = \frac{(E(f_i^{obs}) - E(f_d^{pred}))^2}{\sigma^2}. \tag{18}$$

In addition, the area of each ice shelf region is an order of $10^8 km^2$, which leads to a very large sum of all modelled probabilities between 0 and 0.5 and therefore an extremely large likelihood (note that these values should not be confused with 0 and 1 values set for observed fractures only). In order to achieve a more realistic magnitude of the likelihood function we needed to re-calculate the estimated probabilities by scaling them between 0.55 and 1. To do this we assigned everything below 0.55 the "non-fracture?? value of zero and scaled the remaining values to the range 0 to 1.

For a prior model and prior scores, we took the best-fitting model from the random walk search described above. First, we perform a Bayesian analysis for 500 steps, then narrowed down the selection and accepted only those models that had likelihoods greater than 90% of the best likelihood.

The Cryosphere Discuss., https://doi.org/10.5194/tc-2018-5
Manuscript under review for journal The Cryosphere
Discussion started: 20 March 2018

3.4 Glaciers classification and Jensen-Shannon Divergence (JSD)

In order to select a set of predictors for a general case and find whether it is possible to find a set that can be used for any glacier, we utilised Jensen-Divergence algorithm. We started with the construction of a binary array for each glacier, where the number of rows represents the number of good-fitting models for a glacier and the number of columns represents the 20 predictor factors. Next, we found the average occurrence of each predictor:

$$A_i = \frac{\sum_{j=1}^{N} k_j}{N}, \tag{19}$$

where $i \in [1, 20]$ is the predictor index, N is the number of good-fitting models. $k_j = 1$ when the predictor is included in the good-fit model j and 0 otherwise.

From this we could find how often a certain predictor was included in good-fit models. If a predictor was selected more than 50% of the time then it was assigned as a potential for a best-fit model, otherwise it was set to 0. Thus, we obtained a 34×20 array (34 glaciers vs. 20 predictors) that consisted of 1 when the predictor was included in the best-fit model and 0 otherwise.

Next, we classified the glaciers in groups. There were a large number of possible combinations to select such groups. Therefore, we constructed a test that assessed every possible combination and calculated a percentage of similarity between glaciers in a group (Eq. 20).

$$S = \frac{M}{21} \cdot 100, \tag{20}$$

where M is the number of matches between sets of predictors for two glaciers and S is a group number.

We found that we could categorised all 45 glaciers in 4 different groups, with Group 1 having glaciers that can be more easily combined and Group 4 being a more narrow group of specific glaciers that can not be placed in any of the other three groups.

The JSD can be used as a tool to measure the distance between two distributions and can provide a value that we can use to assign a particular glacier to one of the groups. . The JSD formula is widely used in statistics to measure a divergence of one probability distribution from another. To validate our approach, we applied the additional Jensen-Shannon Divergence method (JSD) to identify the similarity between the best probability for each glacier and a probability calculated by placing the glacier in a certain group The Kullback-Leibler divergence is defined as:

$$JSD(P_1||P_2) = \frac{1}{2}D(P_1||M) + \frac{1}{2}D(P_2||M), \tag{21}$$

where $D(P_1||M) = \sum(P_1 log(P_1/M))$, $D(P_2||M) = \sum(P_2 log(P_2/M))$ are conditional PDFs, $M = \frac{P_1+P_2}{2}$ and P_1, P_2 are

the new probability (when assigning a glacier to a new group) and the old probability (the best-fit model), respectively. Both probabilities P_1 and P_2 have to be normalised before applying Equation 21.

4 Results

4.1 Summary

We applied the LRA method combined with the random walk method to 45 ice shelf regions that include both ice shelves and surrounding grounded ice (the corresponding names and the location can be found in Table 6 and Fig. 2a, respectively) and found a best-fitting model for 44 of them. The fracturing of the other two ice shelves/glaciers cannot be described using the predictors we have, producing unacceptably large or small probabilities. In total, for each ice shelf/glacier the random walk analysis gave a number of possible sets of predictors that can produce a good-fitting model. We combined all of these possible sets for each glacier to see which predictors are always present in the good-fitting model and which ones are never included. The results of the random walk and the Bayesian inversion greed well. Most of the essential predictors for each particular glacier selected in the Bayesian approach were also chosen when performing the random walk. In most cases, the Bayesian analysis showed equal importance of most of the predictors although effective strain rate and velocity had a slightly higher rate of the percentage of selection. There was no universal set of factors that could be used to model all ice shelf regions. However, subsets of glaciers had some similarities in terms of the predictors that had to be included in order to achieve a good-fitting model.

Thus, we assigned the 45 glaciers into 4 groups, requiring that the deviation from the best-fit models did not exceed 5%. After that we performed a test to identify if this selected sets were the optimal choice, by estimating the deviation from the best solution using the Jensen-Shannon Divergence algorithm. We assigned each glacier to a particular group based on its minimum value of the deviation from the best-fitting model in JSD analysis. By doing this we slightly modified the members of each group that we had previously created. For example, Glacier 27 belonged to Group 1 previously and it fit well with only a slight change of the best-fit score. However the JSD showed that if we move this glacier to Group 2 the deviation from the best-fit decreases from 0.01 to 0.003. However, we had to take into account the fact that the JSD algorithm measures the total distance to the best-fit probability and, thus, can decrease the overestimation error but at the same time significantly decrease the success rate (Glaciers 10,13, 15, 11, 30, 32). Therefore, since these six glaciers are of a similar type to the glaciers in Group 1 and their JSD was similar for Group1 and Group 2 (e.g JSD=0.02 in Group 2 and JSD=0.0205 in Group 1) they were assigned to Group 1 to avoid a decrease in the success rate of identifying fractures.

Finally, to reach an optimal agreement between our model and the observations of fractures we assigned each glacier to a particular group and the set of factors for each group are presented in Table 3 and Table 4, 5, respectively. Thus, we found that the sets of predictors for each group varied significantly, however velocity was included in the grounded ice set for all groups. For the floating ice the analysis showed that velocity was not a determining factor in predicting fractures, instead effective strain rate as well as stress principal value was present in each predictor set. The detailed characteristics of each group are described below.

To estimate how well our probability model and the damage model identify observed fractures we calculated the percentage of success and error for each ice shelf/glacier model. First, we found the number of cases when there is a modelled fracture in the vicinity of an observed fracture (within 100-metres radius). Then, we divide this number by the total number of observed fractures and find the percentage of success.

To find the percentage of failure we calculated how many times there is a modelled fracture when there are no observed fractures within a 100-metres radius. We divide this number by the total number of non-fractured nodes to find the failure percentage.

While the success of identifying fractures on floating ice is lower than for grounded ice it was still able to catch the main fracture pattern and the success rate was significantly high for the majority of glaciers see Fig. 1a). Our method is able to identify up to 99% of the exact location of fractures on grounded ice with the average 84% (Figure 1a) and 61% for floating ice (Figure 1b, with a mean overestimation error of 26% and 20%, respectively. There are many cases where our method agrees with the results produced when using the damage-based approach. However, in almost all cases the success of LRA on floating ice was slightly higher than of damage-based method with the exception of two glaciers. Although it is clear that the damage-based method has a relatively high success rate due to the fact, that initially we included nodes with damage over 0.9 to the set of observed fractures, we added damage variable as an additional predictor parameter to glaciers in group 1 and found that it improves the success rate of finding fractures. Overall, for all four groups we can see that in most cases where we could not achieve a high score using LRA, the damage-based method did not produce a high success score either (see Fig. 1b).

4.2 Group 1

This was the largest group of glaciers and the best-fit model includes as many as 10 predictors for grounded ice and seven predictors for floating ice. The analysis of the estimated coefficients in LRA showed that predictors with the highest weights in our model for this group of glaciers were: effective strain rate, proximity to glacier edges and nunataks as well as the surface elevation gradient. We present the modelled probability in Figures 4b and 3c as well as comparison with the damage-based results in Figures 6a and 9c.

The main pattern of surface fractures is well represented for this group. On grounded ice the success of identifying fractures is larger than 88% with a quarter of glaciers at almost 100%. The failure related to overestimation of fractures is 27%. On floating ice the success amounted to 55% and the failure was equal to 15% on average. For Vanderford IS (see Fig. 4b) the overall pattern is well represented, even though high resolution images were not available for this glacier. The overestimation error is mainly related to the region that is far from the ice front and has a relatively high accumulation rate. On floating ice the probability of fracturing is relatively smaller, mainly showing higher chance of fracturing closer to the groundling line. Conversely, Drygalski Ice Shelf has a larger number of high resolution areas and, as a possible result, less overestimation of fracturing (see Fig. 3c). We can see that the "definitely non-fractured nodes" (selected in blue ice areas) are successfully represented in our model. For this glacier none of the observed non-fractured nodes was assigned to have a high probability of fracturing. In most of those nodes the modelled probability was as low as 0.1. Moreover, we can see that in the regions with a large number of observed fractures the probability is as high as 0.9 and it's slightly less in the areas with a lower number of

observed fractures (between 0.6 and 0.8). Although there are observed fractures that were not captured by the model they were not captured by the damage-based model either.

We compared our results to the damage-based approach based on damage inversion and the results for the Cook ice shelf are shown in Fig. 6b. There are distinct fractures visible towards the front of the ice shelf that are not captured by both approaches suggesting that most of them are formed further upstream near the groundling line. It is also possible that the fractures at the central part of the ice shelf are advected from the locations where ice is grounded, which is well represented in the probability-based model. The probability and the damage based models show a good agreement on floating ice.

The modelling results for Larsen B IS are illustrated on Figure 9c. It is clear that the nodes where damage is high have a high probability of fracturing due to the fact that we added damage as one of the predictor parameters to this glacier. It can be also seen that there are two lines of high probability of fracturing that coincide with the location of the large rifts that can be seen on the satellite images.

It is important to note that the results for Nansen IS (Fig. 7c) as well as for Pine Island (Fig. 5a) agree with observations well even though the data from it was not included in the data set used to construct the model. For Pine Island we can observe fractures in the central part of the shelf that were not captured by the model. They were not removed by the damage-based filter as there were no damage upstream on the floating ice. However, our results show that the chance of fracturing upstream where ice is grounded is high, suggesting that the observed fractures are possibly formed at the grounded ice zone.

4.3 Group 2

The second group of glaciers has the best-fit when the bed slope is excluded. Effective strain rate and surface slopes were found to be the most important predictors in the model for this group.

For this group the LRA method predicts fractures with a 70%-90% success on grounded ice and finds about 67% of observed fractures on floating ice with an overestimation of 25% and 27%, respectively. In most cases the model represents the non-fractured nodes with high precision, except for the slight overestimation at the front of the ice shelf. Similar situations are observed for most glaciers in this group: the area of floating ice is relatively small, thus the main prediction is performed for grounded ice. For, example, for Edward VII IS and Rayner Thyner IS (Fig. 3a and 3b, respectively) the modelled probability captures most of the fractured as well as non-fractured nodes on grounded ice with the exception of a few very small regions that are outside of the high resolution image areas.

Interesting results were found for Larsen A IS (see Fig. 4a) showing a very good agreement between our model and the observations. We can see that the nodes observed to be non-fractured and located within the high-resolution regions are also shown to have less chance of fracturing when using LRA method. When comparing the LRA results with the damage-based results for Shirase IS (Fig. 10a) we can see that both methods produce similar results on floating ice, although LRA method captures a slightly higher number of fractures as well as is shows that most of the fractures are formed further upstream on grounded ice.

4.4 Group 3

This group includes 4 ice shelf regions, namely Totten IS, Nivl IS, Dibble IS and Holmes IS. These glaciers were very sensitive to the choice of predictor factors and the JSD process could not assign them to either of the two groups mentioned above. The mean success rate for this group was around 93% with an overestimation rate just above 23% on grounded ice, and 56% and 23% success and error on floating ice, respectively. Interestingly, for Totten only a certain set of factors can produce a good fit to observed fractures. For this glacier, including the back stresses in the model produces a slightly smaller number of modelled fractures. Potentially, in the model for this group we could include the proximity to the ice front since it produces slightly better results for 3 of the 4 glaciers. However, it lowers the success rate for Nivl IS significantly. Thus, in order to achieve a set that would give a good-fitting model for all of the glacier we exclude back stress and the ice front proximity from the list of predictor factors for this group.

In terms of results for Holmes IS (Fig. 7a), there was a good agreement between damage and LRA models as they both were able to predict the main fracture pattern, but LRA captured the observations slightly better, especially at the front of the ice shelf. Similarly, for Dibble IS (Fig. 8c), both methods produced similar pattern, although with a higher overestimation error when using LRA. Nevertheless, LRA method was able to more precisely estimate fractures at the western part of the ice shelf.

Finally, we present the result for the Totten IS (see Fig. 10c). The images we used for this glacier were very hard to interpret due to the presence of many features on the ice surface as well as the low resolution of the imagery. The LRA model as well as Damage model capture most of the fractures we could observe on floating ice, displaying similar distribution patterns. Although, the overestimation is relatively high on grounded ice it is impossible to say if there are no fractures there and our model shows overestimation for this glacier or fractures are not visible due to the low resolution images.

4.5 Group 4

This group includes Larsen C, Amery, George IV and Borchgrevnik IS. The average success and error for this group amounted to 66 and 15 per cent and 56 and 20 per cent for floating and grounded ice, respectively. The most important predictor factors in this group on floating ice are effective strain rate, surface gradient change and thickness, while for prediction of fractures on grounded ice curvature and velocity need to be included in the model. For all of the glaciers in this group we found that including the ice front and grounding line proximity distorts the model, increasing significantly the error due to overestimation of fractures. For Borchgrevnik IS it also leads to a drop of the success rate of fracture prediction. In addition, Larsen C and Amery Ice Shelves can be grouped together but cannot be included in any of the groups mentioned above. For these glaciers only a small number of predictors need to be included in the model. The Bayesian analysis also confirmed the sensitivity of the Amery fracture model to this set of predictor factors. The LRA model for Amery IS (Fig. 5b) was able to capture most of the fracture pattern on the grounded ice and near the edges on floating ice demonstrates a similar pattern to the damage model. For George IV (Fig. 8b) we can observe a very good agreement with observations both on floating and grounded ice. It also shows high probability of fracturing in most location where the high damage zones are predicted. Overall, for both ice shelves we can see that the majority of fractures are formed further upstream from the grounding line.

The Cryosphere Discuss., https://doi.org/10.5194/tc-2018-5
Manuscript under review for journal The Cryosphere
Discussion started: 20 March 2018

5 Glacier Characteristics

5.1 Group 1

The ice shelves/glaciers in this group have a number of characteristics that distinguish them from other ice shelves/glaciers. Most of them are relatively wide with a large floating area. The floating part is not restricted by any channel walls and the width of the shelf is similar to its length. All glaciers in this groups are relatively static, with less curvature or significant surface elevation changes. However, there were two exceptions: Abbot IS and Drygalski IS have slightly different characteristics. First, Abbot is a wide glacier that carries most of the properties of Group 1. However it has a large number of glaciers that restrict its outflow towards the ocean and, therefore, it has similarities with the glaciers from Group 4. This observation is in good agreement with the JSD results that showed that Abbot can be assigned also to Group 4 as the change in JSD distance in this case would be very small. Second, the JSD results showed that Drygalski IS could be as well placed in Group 2 or Group 3. We can see that this ice shelf has some characteristics similar to Group 2 (large number of nunataks) and Group 3 (a very long floating tongue). Therefore, we suggest that some glaciers have mixed features of Group 1-Group 2 (such as Vanderford) or Group 1-Group 3 (Ekström, Tracy-Tremenchus, Rennik), however they still have more characteristics of Group 1 and produce a better-fitting results when assigned to this group.

5.2 Group 2

This group includes a relatively smaller number of ice shelves/glaciers. All of the ice shelves/glaciers have a large amount of nunataks and smaller ice thickness as well as many small narrow channels and fast ice streams. They are mostly located on the Antarctic Peninsula or near the Trans-Antarctic Mountains. All of the ice streams are relatively steep which may explain why it is necessary to include surface slopes in order to achieve a good-fitting probability.

5.3 Group 3

Group 3 glaciers were found to have many similar features. Most of the ice shelf regions have one relatively long glacier that flows inside an embayment. For most of them the glacier length is much higher than the width and they all have a very low glacier channel curvature. The velocities of these ice shelves/glaciers are relatively high which can explain why the changes in strain rate and velocity are the most important predictors for this group.

Interestingly, although the average back stress for Totten IS is one of the highest out of all 34 ice shelf regions, including it in the model does not significantly change the probability of a fracture. Thus, apparently, even having large magnitudes these predictors make just minor contributions to the constructed probability and the other predictors govern the fracture formation for the Totten IS. The effective strain rate is also one of the highest for Totten, but we found that it is not this predictor that mostly contributes to fracture formation, rather it is the effective strain rate gradient. Thus, sudden changes in the flow regime of the glacier would be the most likely cause to promote an increase of the number of fractures.

5.4 Group 4

The JSD analysis has shown that Borchgrevnik IS could also be assigned to Group 1, but it produced slightly better results being placed in Group 4. On the other hand, Amery and Larsen C need to be strictly assigned to Group 4 only. George IV IS and Amery IS have similar characteristics as they are both narrow and long (in fact much longer than any other glaciers of this type in Antarctica) and are located inside an embayment. Furthermore, George IV IS and Larsen C IS are both located next to each other on the Antarctic Peninsula. Although Larsen C IS is not inside an embayment, it is a significantly long and narrow ice shelf stretching around the coast. Borchgrevnik IS also has similar features to the Amery and George IV ice shelves as it is of a similar shape and is located inside a narrow channel. However, it does not have exactly the same characteristics as the other ice shelf regions in this group as it is much shorter, which could be why JSD showed that it can be placed in Group 1.

On the Amery IS (see Fig. 5b) most of the fracturing occurs upstream at the grounding line as well as at the walls of the glacier channel. There were a number of fractures (right hand side of the Fig. 5b, close the the ice front of the glacier) that could not be represented by our models. However, the uncertainty of the fracture observations in this area is high due to the difficulty distinguishing them from the surface features caused by basal crevasses.

Adding the proximity to the grounding line and the ice front did not produce a good fit for the Borchgrevnik IS because of the specific shape of this region. The distance between the front and the grounding line is very small relatively to other glaciers in our analysis.

5.5 Discussion

We found that, in general, the most important predictor factors to model fractures for all analysed glaciers on grounded ice were velocity and variations of the surface gradient, which is in agreement with the theory of possible mechanism of fracture formation (Colgan et al., 2016). Interestingly, the required parameters on floating ice were different, with effective strain rate and principal stress being the most important. In addition, previous analysis based on damage accounts for effective stresses, thickness and viscosity, but does not include such predictors as proximity to glacier edges, nunataks and the grounding line as well as the curvature of a channel, which helped to improve the modelling of the fracture formation on most ice shelves in our analysis. Our results can be used in Antarctic logistics in order to determine snow covered crevasses as they can be a potential hazard for navigation in Antarctica. Many researchers use ground penetrating radar to find hidden crevasse, but it is a real time assessment method that requires both financial and human resources and, therefore, can not cover all the areas in Antarctica. Our approach can be done remotely and at low cost, in advance of field campaigns.

We do not claim that all the predictors that were chosen in the final set for each group represent the exact fracture mechanism for each glacier. We can see that, for some glaciers, sets containing different predictors can lead to results close to the best-fitting model. However, for some cases such as Amery and Totten Ice Shelves the number of good-fitting models is very limited. For example, including the friction coefficient and proximity to the ice front in the analysis we can achieve a better fit to the observations. Therefore, we conclude that some factors have a very strong effect on fracture formation process and some

still have an effect but it is minor for some glaciers. Ultimately, we seek only to be able to develop a model that can identify correctly the geographical location of fractures, not necessary explain why they are there.

The main uncertainty of our method comes from the overestimation of the number of fractures. We do not know how many fractures are not visible on satellite images as well as it is not certain if the damage-method with given parameters can predict fractures for any given ice shelf, therefore it is uncertain what overestimation rate we should allow in our model. A possible solution to this could be to supplement satellite images with radar and seismic measurements (Navarro et al., 2005; Delaney and Arcone, 2005) or to acquire higher resolution satellite images that can help to identify location of fractures even if they are hidden under the snow surface. However, for our method it would require a large set of observational data. In our paper we assume that 20-25% rate of over-estimation should be reasonable. We can see that most of our results show overestimation of fracture formation in the areas around observed fractures. This shows as well that our overestimation might be reasonable as fractures are more likely to be formed if there are other fractures already present nearby. Our assumption is based on the fact that the ice regime conditions are similar within a 500 metres radius, not implying any direct influence of the old fractures to the new fractures (Colgan et al., 2016). In addition, the area of high probability of a fracture is larger than the number of observed fractures mainly due to the fact that it is impossible to select all of the fractures on the satellite images manually. The selected observed fractures capture the main areas of fracturing assuming that surrounded nodes are likely to be fractured as well.

The overestimation of the fracturing in the case of Vanderford (see Fig. 4b) can be seen mainly at the front of the ice shelf. There is a very high chance of developing surface fractures in that area and therefore it might be that the fractures are just not yet visible on the satellite images. In fact, that region has a relatively high snow accumulation rate reaching 1 m/yr. After closer inspection of the satellite image areas where we see the over-estimation error, we can recognise the presence of surface fractures but, due to a very large number of fractures around Antarctica, the manual selection of all the fractured data points is a time intensive process. Sampling with a higher spatial density would require an automated algorithm. However, it is important to note that the low spatial density sampling does not influence the results of the fracture probability (as mentioned previously only diversity in sampling is important), it affects only the observations data set that we use to estimate the success of our model. Thus, under-identification of fractures can lead to an apparent overestimation of the error.

The damage-based approach sometimes produces areas of high damage downstream from the observed fractures (Fig. 8d). If we assume that there are some fractures that are invisible on the images it is still unclear why the modelled ice is not damaged upstream where observed fractures are present. If we could see damaged ice upstream from the observed fractures we could assume that the ice was damaged and transported downstream where we can see fractures. However, in many results based on the damage approach we could not identify this type of behaviour. Even after correcting the observations of fractures by back integrating the flow of ice, we still can find fractures that do not have zones of high damage downstream. In addition, the method based on damage inversion predicts only damage on floating ice, whereas fractures are often formed upstream from the grounding line. In the probability-based model this type of behaviour accounts for and in most cases overestimation of fractures occurs in a vicinity or upstream from observed fractures. In Figure 7a we show modelled probability of fracturing for Holmes IS. We can see that the overestimation rate is quite small and it all occurs upstream from the observed fractures,

which might be due to fractures that were formed further upstream being transported downstream where they are invisible on the satellite images.

We looked at various properties of the ice shelves/glaciers for which we could not find a good approximation using any of the 19 predictors (part of the Ronne IS, for example) . We found that some estimated predictors had extreme values. For example, we found that rheology of Larsen B is the lowest out of all glaciers in our analysis; the ice thickness and proximity to the grounding line were the smallest. Furthermore, it has the highest strain rate change as well as the highest surface elevation change. On the other hand, Ronne IS has the lowest elevation change as well as the principal stresses components. We do not have enough samples to cover values that are non-typical for the majority of glaciers, which might be the reason we could not find a good-fit model for these two glaciers. The analysis of these two ice shelves/glaciers using Bayesian analysis produced similar results, confirming that including any of the 19 predictors do not produce a good likelihood in those regions. Thus, we conclude that our probabilistic model is not appropriate for these two glaciers.

6 Conclusions

Most previous large scale modelling of fracture formation has been focused on applying Continuum Damage Mechanics. However, we have shown that, using the suggested nominal parameters this approach does not fully reproduce the nature of fracturing for any ice shelf region and the location of fracture formation sometimes has a large error. In this study we looked at this problem from a different perspective by constructing a probabilistic model based on the observations of surface fractures. The main advantage of the method is that it can model fractured zones not only on floating ice but also on grounded ice.

We found that Logistic Regression Analysis combined with other statistical methods can significantly improve the prediction of fracture formation for the Antarctic ice shelves/glaciers and can lead to the identification of up to 99% of observed surface crevasses for some ice shelf regions with an average of 70% for all ice shelf regions. Our approach has a number of uncertainties and leads to some overestimation of the number of fractures in comparison to the observations, but the rate is not significantly higher than the overestimation error found when using the damage-based method. However, damage-based method helped to significantly improve the quality of the observations of fractures, allowing to distinguish between zones where fractures initiated and zones where they were advected, although location of many fractures did not have modelled damage downstream suggesting an underestimation when applying the damage method, it is possible that damage-based method needs to be tuned for every ice shelf separately.

We classified the Antarctic ice shelf regions into 4 groups. Each group has a set of factors that can be used in the Logistic Regression Analysis to estimate the probability of fracturing in a certain location. We also found that the ice shelves/glaciers in each group have similar characteristics. There were ice shelves/glaciers of specific shapes and having specific regimes that are more difficult to describe applying the general set of factors suggested in this study. However, overall our method can work as a tool that can be efficiently used in the analysis of fracture formation for most of the ice shelves/glaciers in Antarctica.

Our model is easy to implement and can be effectively used as a basis and first step in implementing a calving parameterization in ice sheet models. Being able to accurately predict zones of formation of small fractures provides the basis for modelling

The Cryosphere Discuss., https://doi.org/10.5194/tc-2018-5
Manuscript under review for journal The Cryosphere
Discussion started: 20 March 2018

of fracture propagation at the locations where we determine fractures using LRA. This can then lead to an implementation of a calving parameterization. Thus, this statistics-based method can help to expand our current knowledge of the crevasses as well as improve mapping of potential hazards.

7 Tables

Table 1. Development of calving parameterisations

Year	Reference	Method
1955	Crevasse penetration depth using tensile stress and overburden pressure	Nye (1955)
1973	Crevasse penetration depth of a single crevasse	Weertman (1973)
1976	Crevasse penetration depth estimation using LEFM	Smith (1976)
1993	Strain related fracture formation	Vaughan (1993)
1997	Sea level dependent calving	Motyka (1997)
1998	Linear Elastic Fracture Mechanics	Van der Veen (1998a, b)
2003	Damage mechanics for a single crevasse	Pralong et al. (2003)
2005	Damage mechanics for a single crevasse	Pralong and Funk (2005)
2007	Crevasse depth	Benn et al. (2007a, b)
2010	Crevasse depth	Nick et al. (2010)
2010	Crevasse depth	Otero et al. (2010)
2012	Damage mechanics applied to a crevasse field	Borstad et al. (2012)
2012	Kinetic 1st order calving	Levermann et al. (2012)
2012	CDM	Duddu and Waisman (2012)
2013	CDM	Duddu and Waisman (2013)
2013	Discrete element models	Bassis and Jacobs (2013)
2013	Particle-based simulation	Astrom et al. (2013)
2013	Crevasse depth criterion	Nick et al. (2013)
2014	Crevasse depth criterion	Cook et al. (2014)
2014	CDM	Albrecht and Levermann (2014)
2014	Combining CDM and LEFM	Krug et al. (2014)
2016	von Mises tensile stress	

The Cryosphere Discuss., https://doi.org/10.5194/tc-2018-5
Manuscript under review for journal The Cryosphere
Discussion started: 20 March 2018

Table 2. Predictor factors (predictors)

Type	Predictor	Description
Geometry	Ice thickness	Bedmap2 data for Antarctica at 1 km spatial resolution
	Maximum bed slope	Bedrock and ice surface slopes are calculated using a nodal function
	Maximum surface slope	
	Surface slope gradient	Maximum slope change in a 400-600 metres vicinity
	Proximity to the ice front	$\mathbf{DM_{IF}}$, calculated using Eq. 8
	Proximity to grounding line	$\mathbf{DM_{GL}}$, calculated using Eq. 9
	Proximity to glacier edges and nunataks	
	Curvature	Curvature of the glacier channel α, calculated in each node based on the direction and rate of the flow velocities (see Eq. 10)
Flow parameters	Backstress	Buttressing effect on ice streams calculated in ISSM from inversion
	Velocity	InSAR ice flow velocity
	Rheology predictor (viscosity)	B, Glen's flow predictor, calculated from inversion of velocities (only for floating ice)
	Friction coefficient	calculated from inversion of velocities
	Effective Strain rate	The effective strain rate is calculated using Eq. 6 with observed velocities as an input
	Principal stress (1 and 2)	Eigenvalues λ (normal stresses) in Eq. 5
	Principal strain rate (1 and 2)	Eigenvalues μ (see Eq. 7)
	Strain rate gradient	Maximum strain rate change in a 400-600 metres vicinity

The Cryosphere Discuss., https://doi.org/10.5194/tc-2018-5
Manuscript under review for journal The Cryosphere
Discussion started: 20 March 2018

Table 3. Formed groups of ice shelf regions

Group1	9, 10, 11, 12, 13, 15, 18, 20, 21, 23, 25, 26, 30, 31, 32, 34, 4, 29
Group2	3, 6, 7, 8, 19, 27, 28, 33, 35
Group3	14, 17, 22, 24
Group4	1, 2, 5, 16

Glaciers/ice shelves for which we could not find a good-fitting probability are marked with red.

Table 4. Predictors for grounded ice regions in each formed group

	Effective stress	Effective strain rate	Principal 1 strain rate	Principal 2 strain rate	Principal 1 stress	Principal 2 stress	Surface slope	Bed slope	Strain change	Curvature	Friction coefficient	Rheology B	Thickness	at the ice front	at the grounding line	near edges	surface change	Velocity
Group1:		✓	✓				✓			✓		✓		✓		✓	✓	✓
Group2:	✓				✓				✓		✓	✓	✓				✓	✓
Group3:				✓							✓		✓			✓		✓
Group4:		✓							✓	✓							✓	✓

Tick-mark stands for an addition of a predictor to the model for grounded ice.

Table 5. Predictors for floating ice in each formed group

	Effective stress	Back stress	Effective strain rate	Principal 1 strain rate	Principal 2 strain rate	Principal 1 stress	Principal 2 stress	Surface slope	Strain change	Curvature	Rheology B	Thickness	at the ice front	at the grounding line	surface change	Velocity
Group1:	✓				✓	✓		✓	✓							✓
Group2:			✓			✓					✓	✓		✓	✓	
Group3:			✓				✓				✓	✓			✓	
Group4:		✓	✓	✓				✓	✓					✓	✓	✓

Tick-mark stands for an addition of a predictor to the model for floating ice.

The Cryosphere Discuss., https://doi.org/10.5194/tc-2018-5
Manuscript under review for journal The Cryosphere
Discussion started: 20 March 2018

Table 6. A list of analysed ice shelf regions

Glacier	Group	Corresponding IS name	Region
1	4	George IV	Palmer land, AP
2	4	Larsen C	Fallieres Coast, AP
3	2	Larsen D	Black Coast, AP
4	1	Orville Coast side of the Ronne IS	WA
5	4	Amery	EA
6	2	Edward VII	Mawson Coast, EA
7	2	Rayner Thyner	EA
8	2	Shirase	Prince Harald Coast, EA
9	1	Stancomb-Brunt	Caird Coast, EA
10	2	Riiser-Larsen	Princess Martha Coast, EA
11	3	Fimbul IS	EA
12	1	Abbot	Eights Coast, WA
13	2	Baudoin	Princess Ragnhild Coast, EA
14	3	Nivl	Princess Astrid Coast, EA
15	1	Borchgrevnik and Lazarev	Princess Astrid Coast, EA
16	4	Borchgrevnik	Princess Raghild Coast, EA
17	3	Dibble IS	Clarie Coast, EA
18	1	Mertz IS	EA
19	2	Rennik	Pennell Coast, EA
20	1	Cook	George V Coast, EA
21	1	Ninnis	George V Coast, EA
22	3	Holmes	Banzare Coast, EA
23	1	Moscow University	Sabrina Coast, EA
24	3	Totten IS	EA
25	2	Vanderford IS	EA
26	1	West IS	Queen Mary Coast, EA
27	2	Larsen C	Oscar II Coast, AP
28	2	Larsen B	Nordenskjold Coast, AP
29	2	Larsen A	Davis Coast, AP
30	3	Tracy-Tremenchus	Knox Coast, EA
31	1	Drygalski	Scott Coast, EA
32	2	Mariner	Borchgrevnik Coast EA
33	3	Rennik	Lazarev Mountains, Oates Coast, EA

The Cryosphere Discuss., https://doi.org/10.5194/tc-2018-5
Manuscript under review for journal The Cryosphere
Discussion started: 20 March 2018

Table 7. A list of analysed ice shelf regions

Glacier	Group	Corresponding IS name	Region
34	1	Filchner	Coast Land, WA
35	2	Ross East	Hut Point Peninsula, EA
36	1	Wilkins and George VI	Rumill Coast, AP
37	1	Stange and Ferringo IS	Bryan Coast, AP
38	1	Pain Island and Thwaites	Walgreen Coast, WA
39	2	Getz	Hobbs and Bakutis Coast, WA
40	1	Nickerson and Sulzberger	Ruppers Coast, WA
41	1	West	Leopold and Astrid Coast, EA
42	1	Jelbart and Atka	Princess Martha Coast, WA
43	1	Nansen	Borchgrevnik Coast, EA
44	1	Prince Harald	Prince Harald Coast, EA
45	1	Larsen B	Oscar II Coast, AP

AP - Antarctic Peninsula, EA - East Antarctica, WA - West Antarctica, IS -ice shelf

The Cryosphere Discuss., https://doi.org/10.5194/tc-2018-5
Manuscript under review for journal The Cryosphere
Discussion started: 20 March 2018

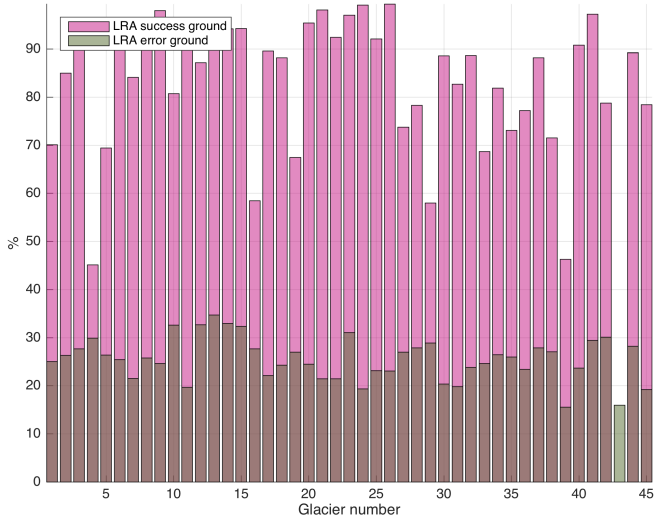

(a) Success and Error

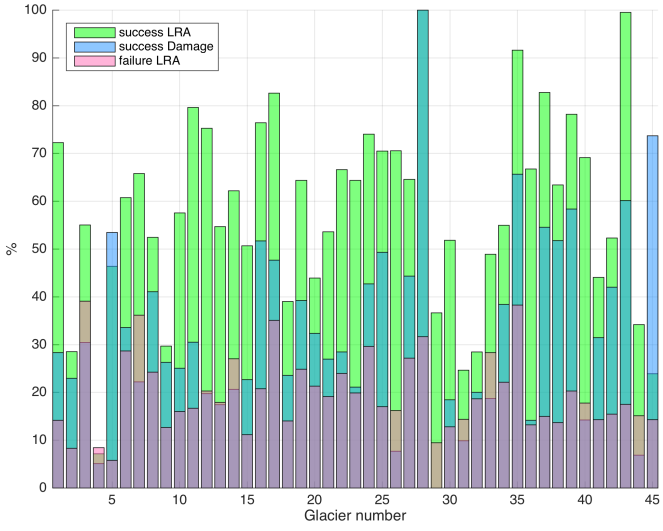

(b) Location

Figure 1. Success and error percentages for LRA for grounded ice is shown in panel a. Results for the floating ice applying LRA vs. Damage method is shown in panel b.

The Cryosphere Discuss., https://doi.org/10.5194/tc-2018-5
Manuscript under review for journal The Cryosphere
Discussion started: 20 March 2018

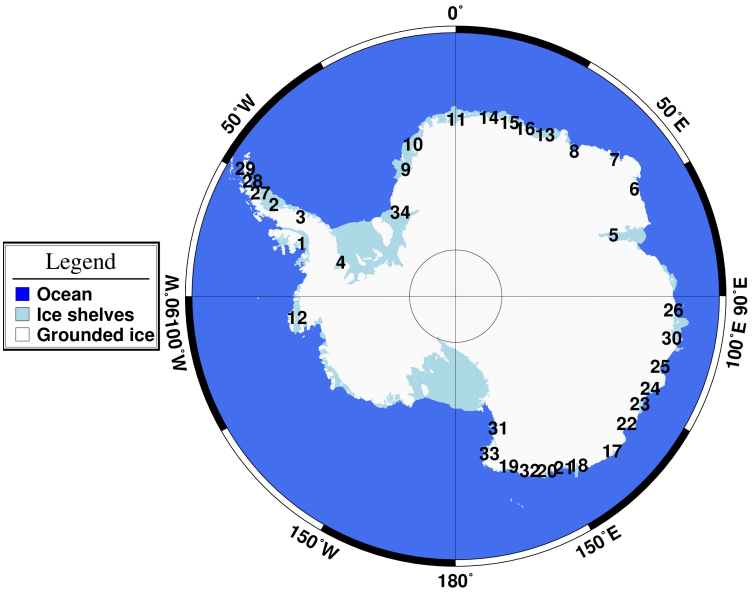

(a) Location

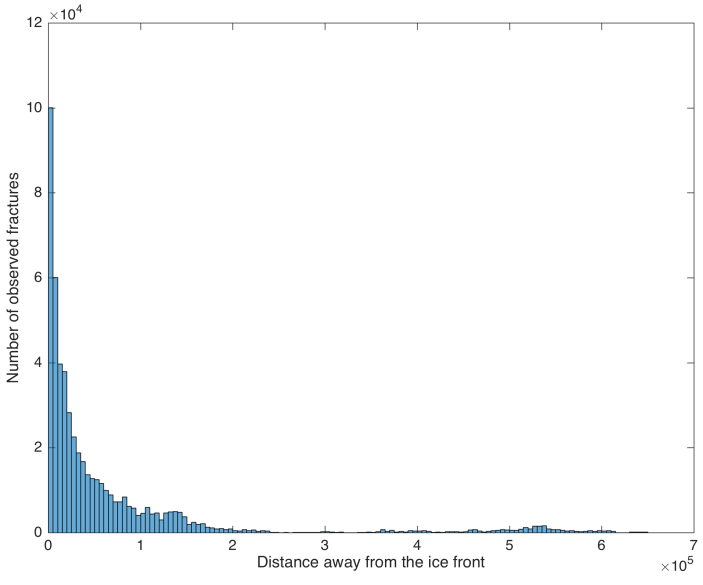

(b) Distance to the ice front

Figure 2. The location of each of the 45 ice shelf regions is shown in panel a. The number of observed fractures versus distance from the ice front (b).

The Cryosphere Discuss., https://doi.org/10.5194/tc-2018-5
Manuscript under review for journal The Cryosphere
Discussion started: 20 March 2018

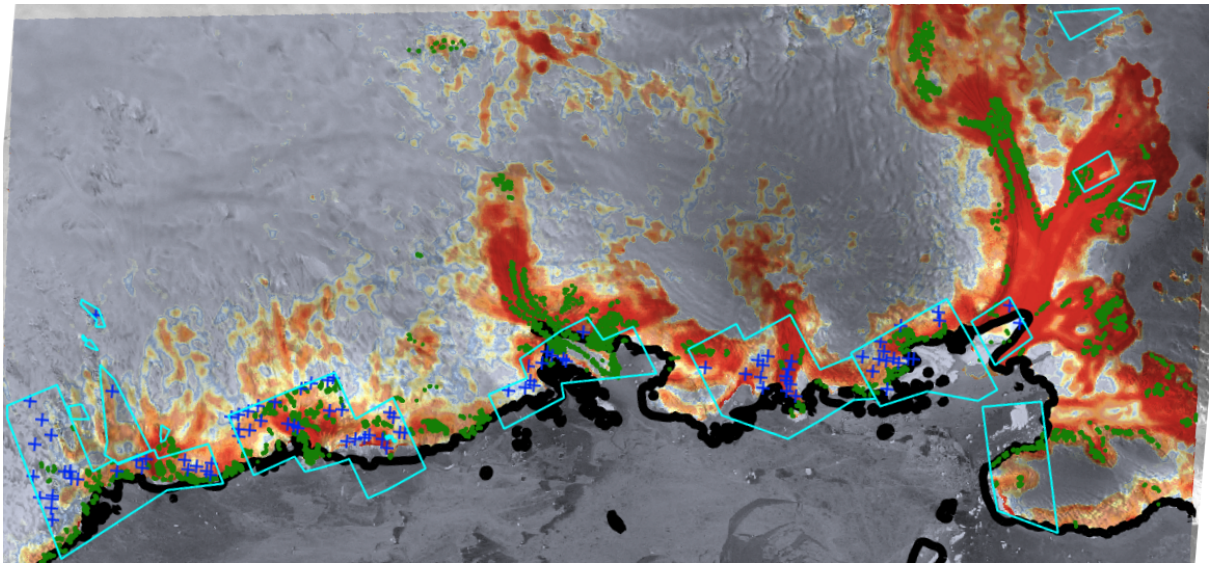

(a) Edward VII IS, Group 2

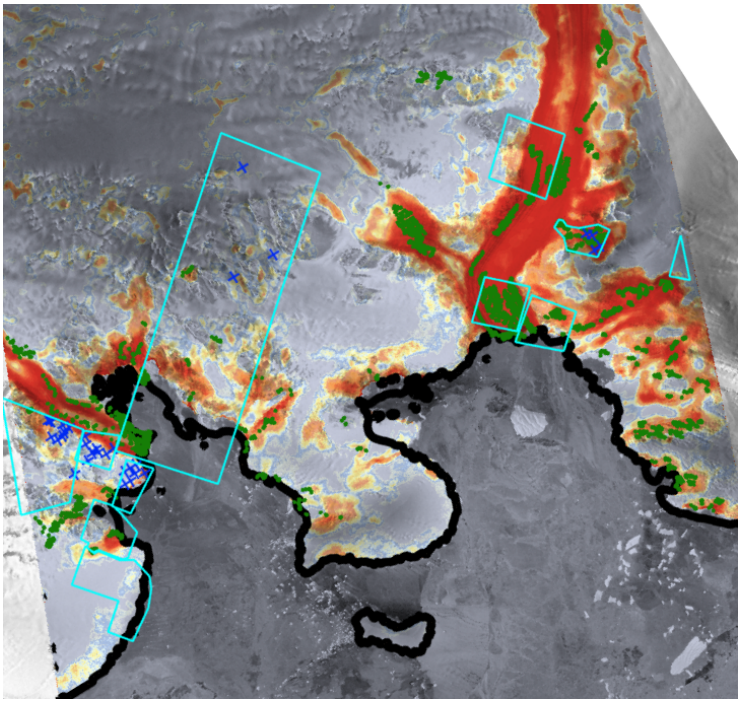

(b) Rayner Thyner IS, Group 2

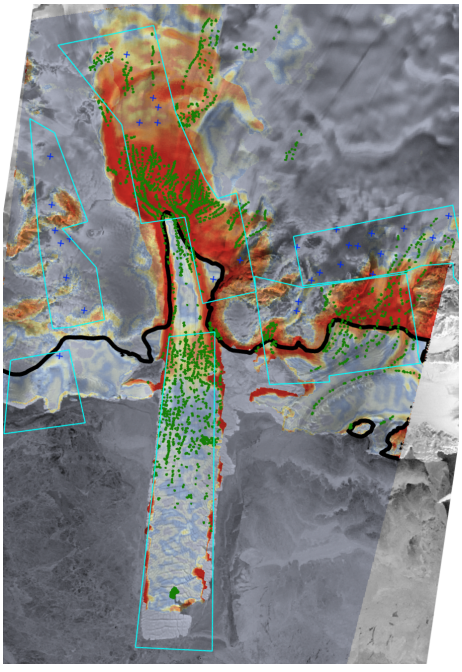

(c) Drygalski IS, Group 1

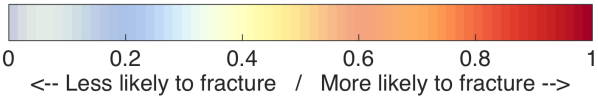

Figure 3. Modelled probability of a fracture for Group 2: Rayner Thyner IS (a) and Edward VII IS (b) and Group 1: Drygalski IS (c) . Observed surface fractures are shown in green and observed non-fractured ice is marked with blue crosses. Light blue polygons represent regions where high resolution images were available. Black solid line shows the location of the grounding line.

The Cryosphere Discuss., https://doi.org/10.5194/tc-2018-5
Manuscript under review for journal The Cryosphere
Discussion started: 20 March 2018

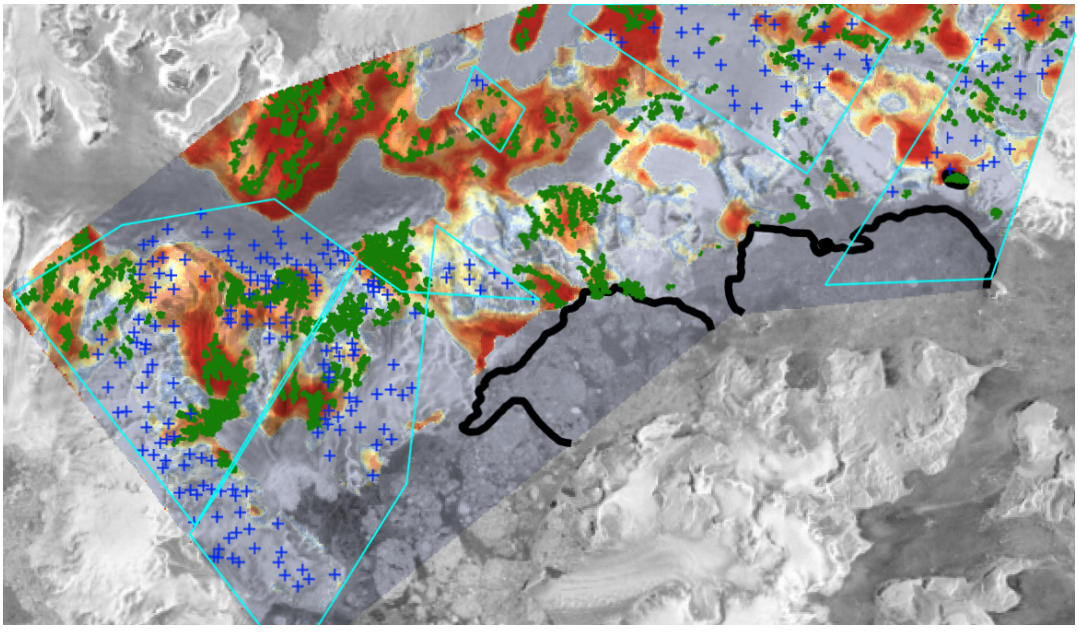

(a) Larsen A, Group 2

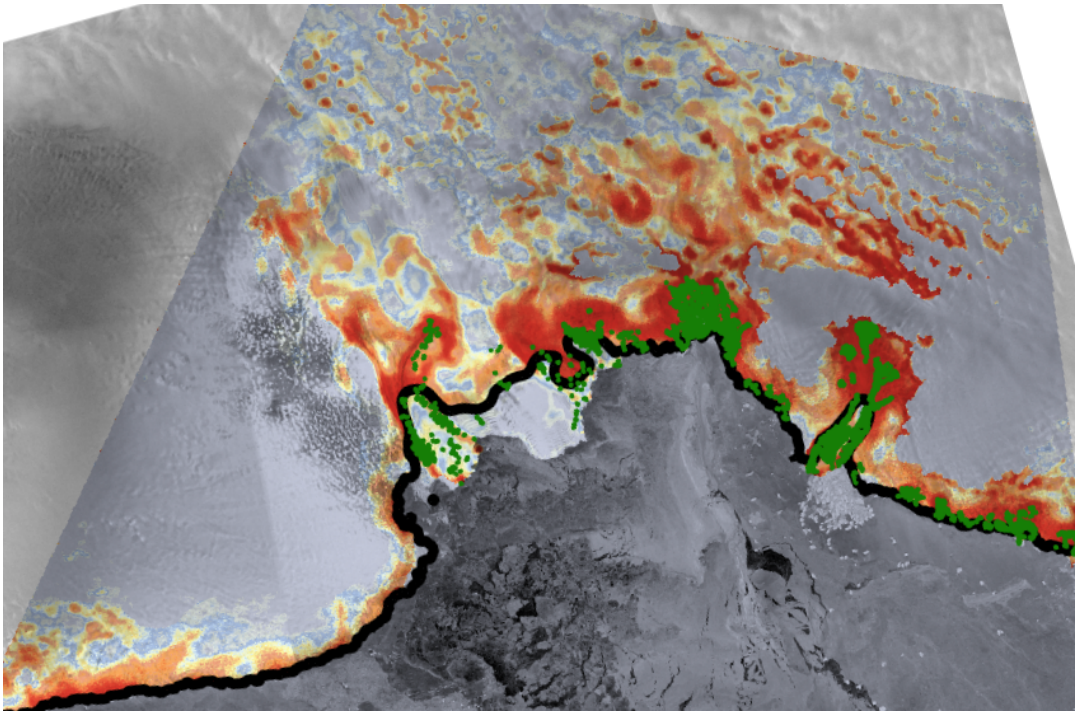

(b) Vanderford IS, Group 1

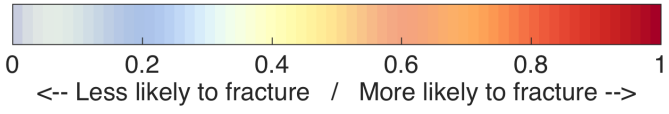

Figure 4. Modelled probability of a fracture for Group 2: Larsen A IS (a) and Group1: Vanderford IS (b). Labels the same as Fig. 3.

The Cryosphere Discuss., https://doi.org/10.5194/tc-2018-5
Manuscript under review for journal The Cryosphere
Discussion started: 20 March 2018

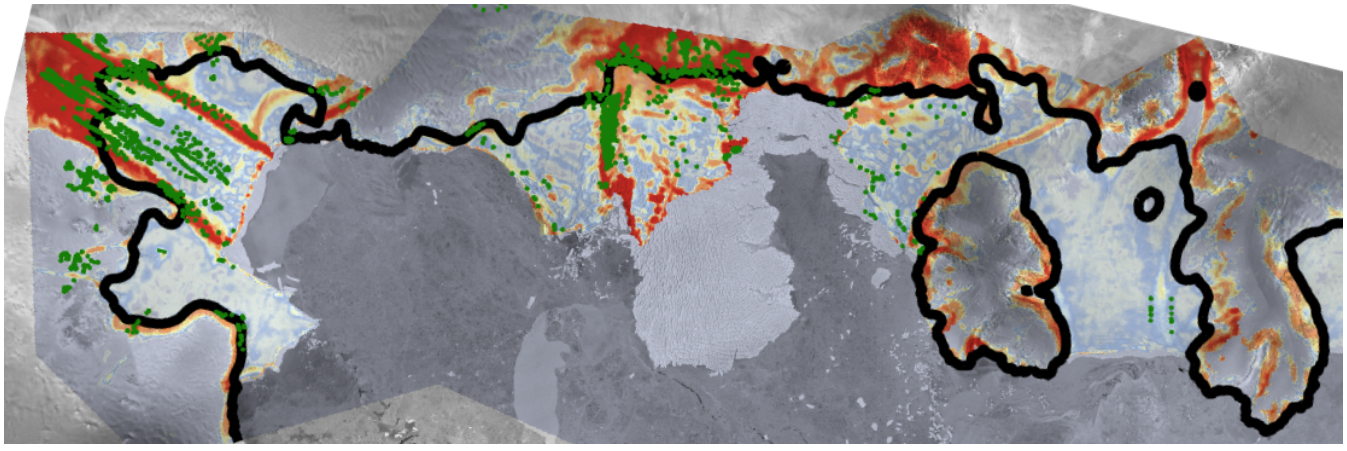

(a) Pain Isalnd and Thwaites, Group 1

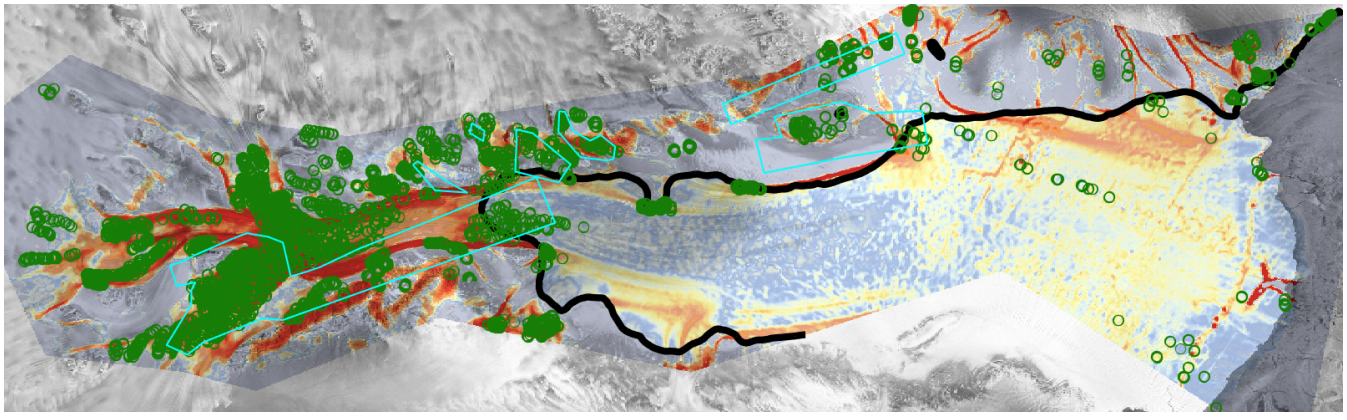

(b) Amery IS, Group 4

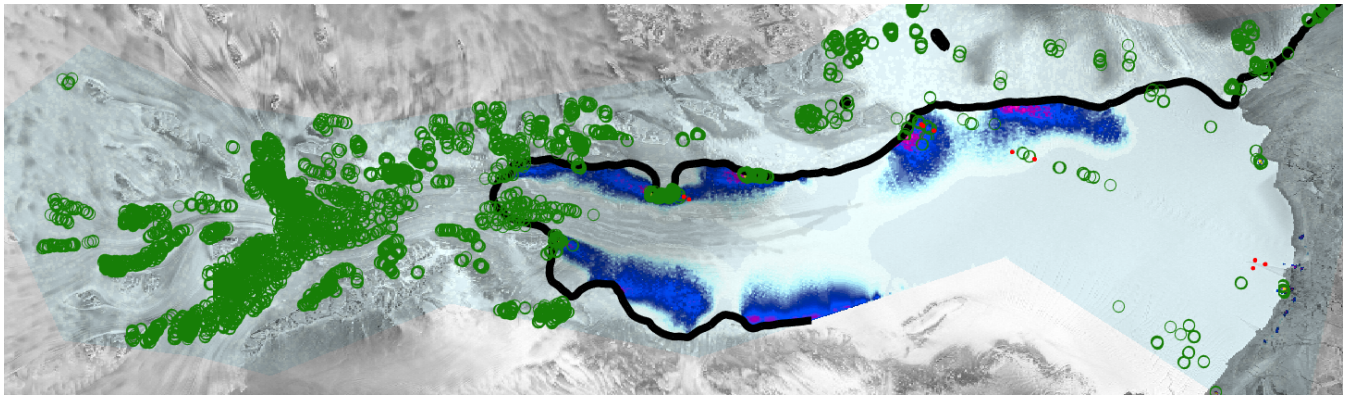

(c) Amery IS, Group 4

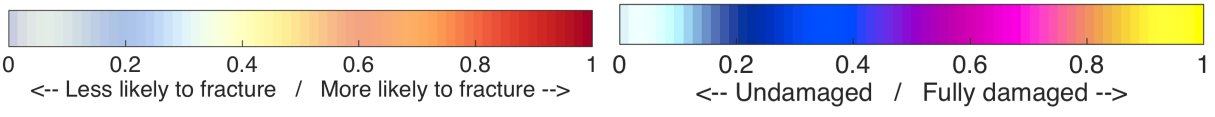

Figure 5. Modelled probability for Pain Island (Group 1) (a) and modelled probability and damage for Amery IS (Group 4) (b,c). Labels the same as Fig. 3.

The Cryosphere Discuss., https://doi.org/10.5194/tc-2018-5
Manuscript under review for journal The Cryosphere
Discussion started: 20 March 2018

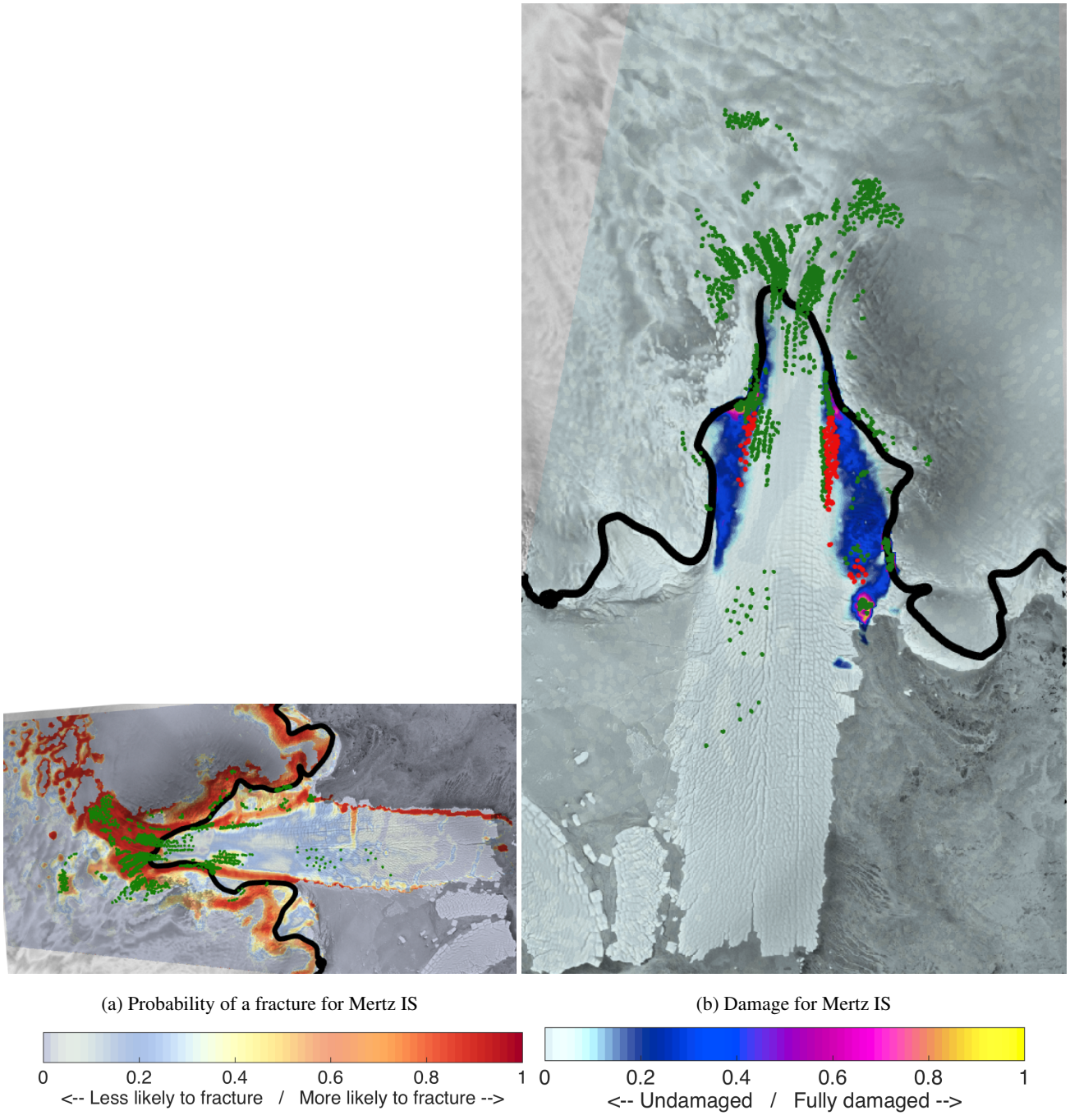

(a) Probability of a fracture for Mertz IS

(b) Damage for Mertz IS

Figure 6. Modelled probability (Fig. a) and damage (Fig. b) at Mertz IS (Group 1). Labels the same as Fig. 3. In figure b the red dots represent the observed fractures that were filtered out due to damage upstream.

The Cryosphere Discuss., https://doi.org/10.5194/tc-2018-5
Manuscript under review for journal The Cryosphere
Discussion started: 20 March 2018

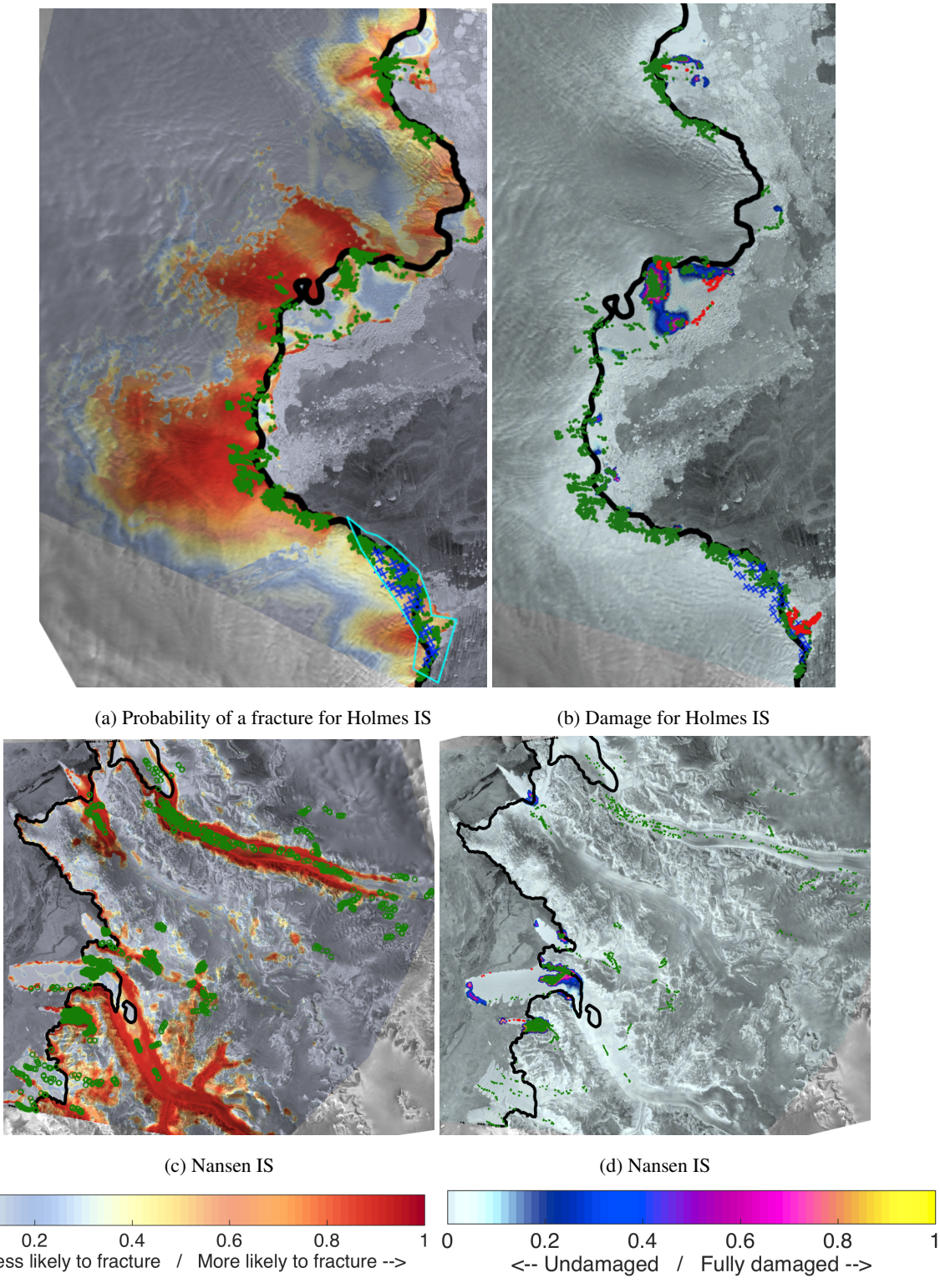

Figure 7. Modelled probability of a fracture vs. modelled damage for Holmes IS (Group 3) (a, b) and Nansen IS (Group 1) (c, d). Labels are the same as in Fig. 3 and 6.

The Cryosphere Discuss., https://doi.org/10.5194/tc-2018-5
Manuscript under review for journal The Cryosphere
Discussion started: 20 March 2018

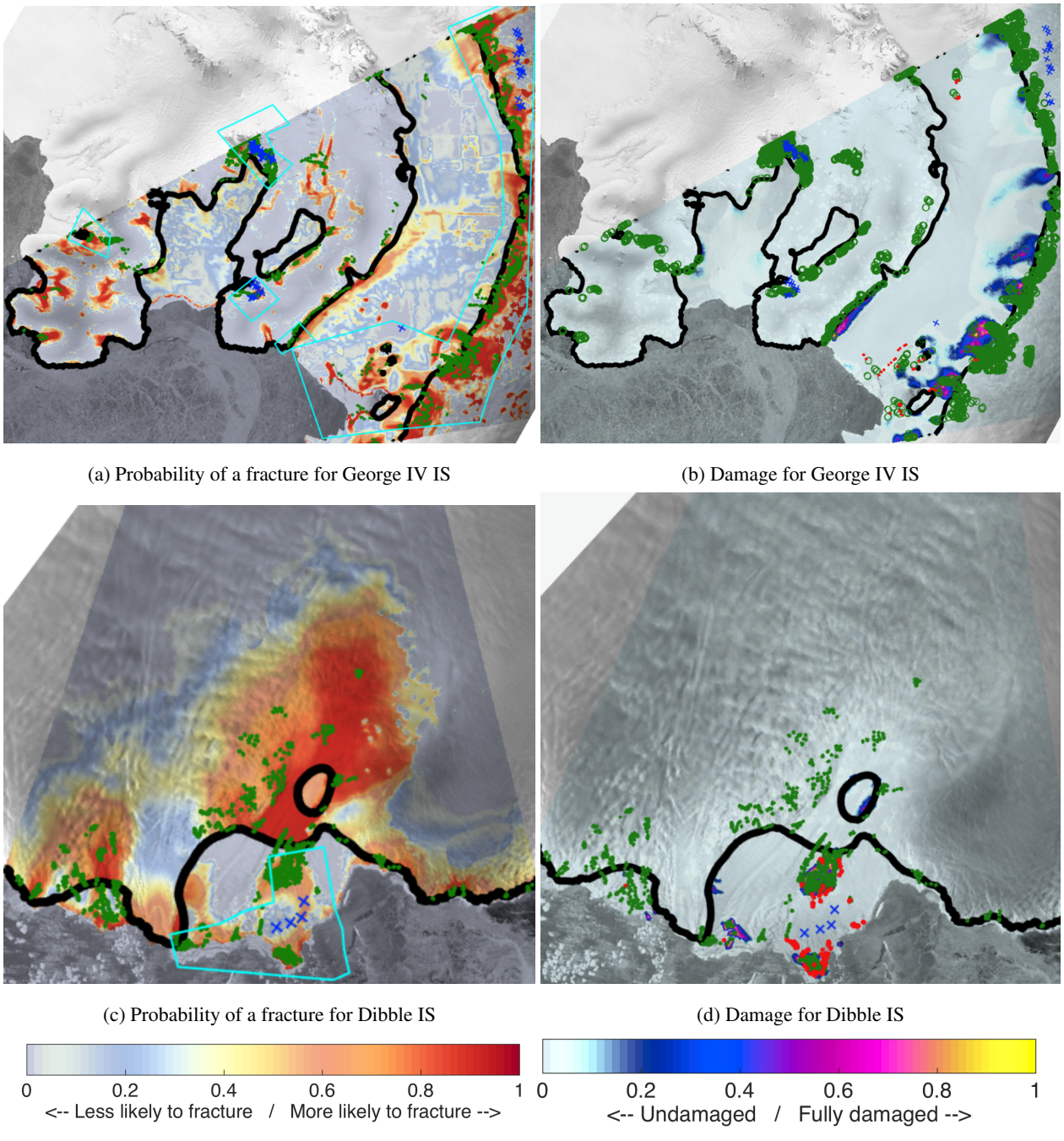

(a) Probability of a fracture for George IV IS

(b) Damage for George IV IS

(c) Probability of a fracture for Dibble IS

(d) Damage for Dibble IS

Figure 8. Modelled probability of a fracture vs. modelled damage for George IV IS (Group 4) (a, b) and Dibble IS (Group 3) (c, d). Labels are the same as in Fig. 3 and 6.

The Cryosphere Discuss., https://doi.org/10.5194/tc-2018-5
Manuscript under review for journal The Cryosphere
Discussion started: 20 March 2018

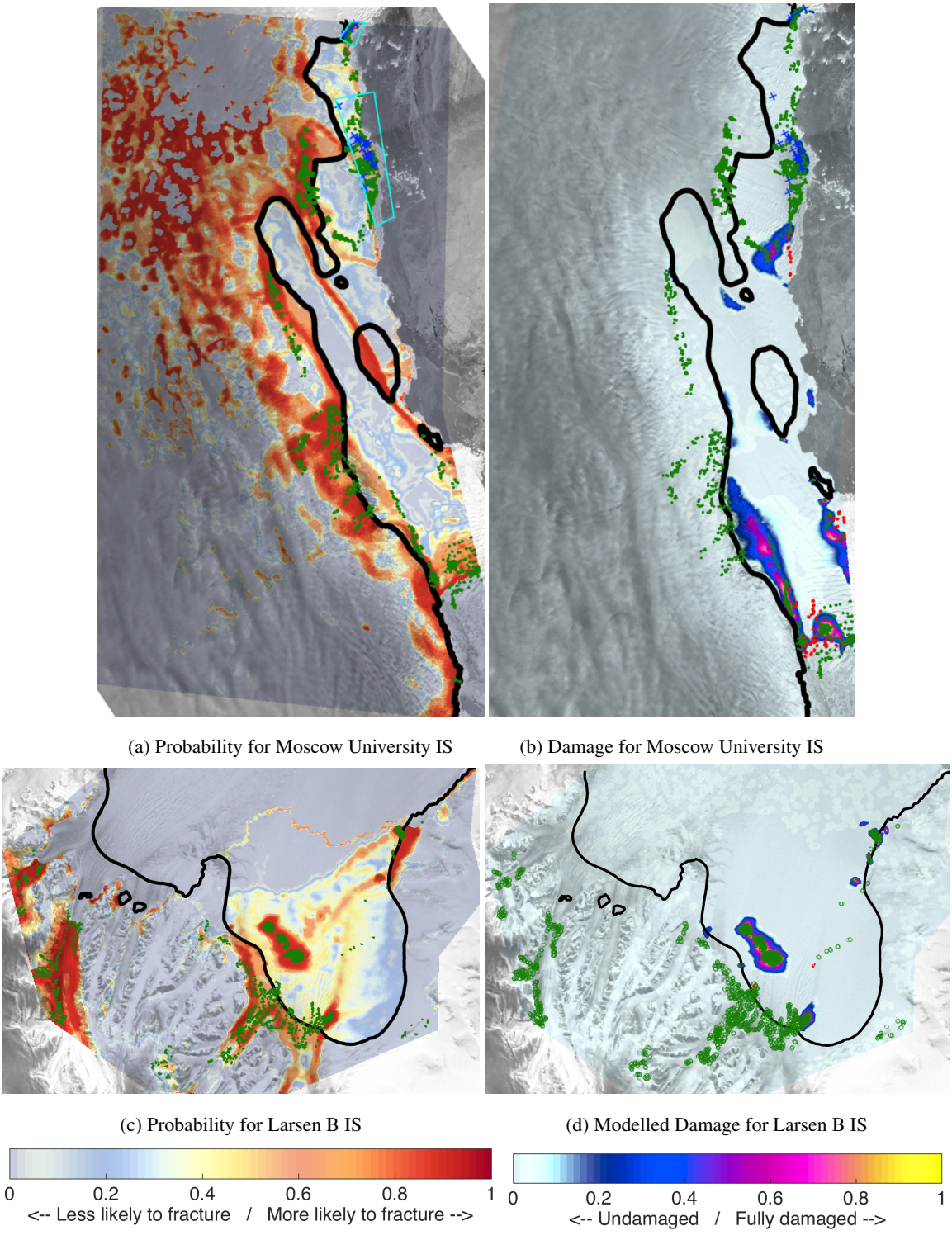

(a) Probability for Moscow University IS (b) Damage for Moscow University IS

(c) Probability for Larsen B IS (d) Modelled Damage for Larsen B IS

Figure 9. Modelled probability of a fracture vs. modelled damage for Moscow University IS (Group 1) (a, b) and Larsen B IS (Group 1) (c, d). Labels are the same as in Fig. 3 and 6

The Cryosphere Discuss., https://doi.org/10.5194/tc-2018-5
Manuscript under review for journal The Cryosphere
Discussion started: 20 March 2018

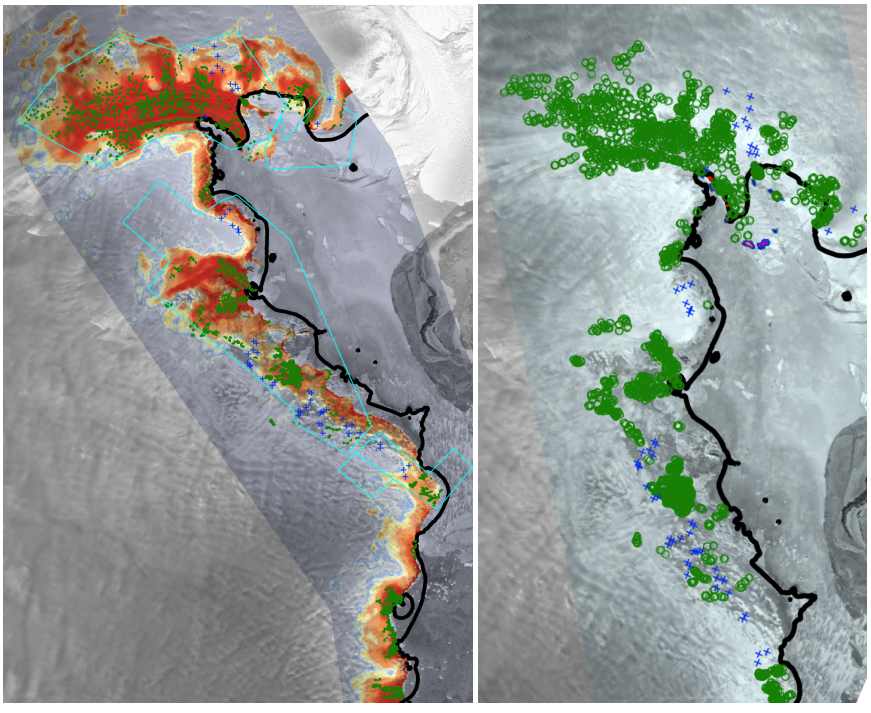

(a) Probability of a fracture for Shirase IS (b) Modelled Damage for Shirase IS

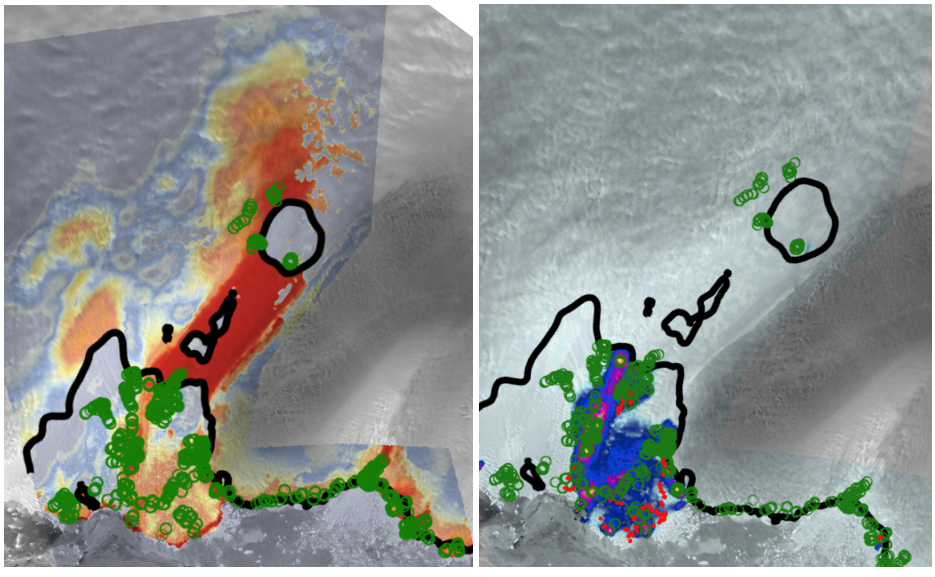

(c) Probability of a fracture for Totten IS (d) Damage for Totten IS

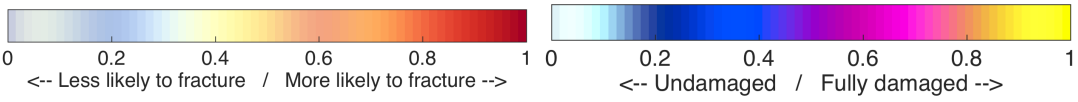

Figure 10. Modelled probability of a fracture vs. modelled damage for Shirase IS (Group 2) (a, b) and Totten IS (Group 3) (c, d). Labels are the same as in Fig. 3 and 6 .

Author contributions. Veronika Emetc designed the study, developed the methodology, collected the data, performed the analysis, and wrote the manuscript. Paul Tregoning helped with models and revising the manuscript significantly. Mathieu Morlighem helped with the implementation of the analysis in ISSM, development of the code, implemented some features needed for the model and helped revising the manuscript. Chris Borstad suggested a way to improve the observational set using the damage-based results as well as helped with the damage description and modelling. Malcolm Sambridge developed the source function for the Bayesian analysis.

Acknowledgements. We would like to thank Teresa Neeman for her help with Logistic Regression Algorithm. We are also grateful to Anthony Purcell for his always helpful advices. Veronika Emetc received scholarship from ARC Discovery DP140103679. We would like to thank Julian Byrne for his help with setting up the ISSM software on Terrawulf.

References

Albrecht, T. and Levermann, A.: Fracture-induced softening for large-scale ice dynamics, The Cryosphere, 8, 587, 2014.

Alley, K. E., Scambos, T. A., Siegfried, M. R., and Fricker, H. A.: Impacts of warm water on Antarctic ice shelf stability through basal channel formation, Nature Geoscience, 9, 290–293, 2016.

Alley, R. B., Horgan, H. J., Joughin, I., Cuffey, K. M., Dupont, T. K., Parizek, B. R., Anandakrishnan, S., and Bassis, J.: A simple law for ice-shelf calving, Science, 322, 1344–1344, 2008.

Astrom, J., Riikila, T., Tallinen, T., Zwinger, T., Benn, D., Moore, J. C., and Timonen, J.: A particle based simulation model for glacier dynamics, Cryosphere, 2013.

Bassis, J. and Jacobs, S.: Diverse calving patterns linked to glacier geometry, Nature Geoscience, 6, 833–836, 2013.

Bassis, J. N. and Ma, Y.: Evolution of basal crevasses links ice shelf stability to ocean forcing, Earth and Planetary Science Letters, 409, 203–211, 2015.

Benn, D. I. and Evans, D. J. A.: Glaciers and Glaciation, Hodder Education, An Hachette UK Company, 2010.

Benn, D. I., Hulton, N. R., and Mottram, R. H.: 'Calving laws','sliding laws' and the stability of tidewater glaciers, Annals of glaciology, 46, 123–130, 2007a.

Benn, D. I., Warren, C. R., and Mottram, R. H.: Calving processes and the dynamics of calving glaciers, Earth-Science Reviews, 82, 143–179, 2007b.

Borstad, C., Khazendar, A., Larour, E., Morlighem, M., Rignot, E., Schodlok, M., and Seroussi, H.: A damage mechanics assessment of the Larsen B ice shelf prior to collapse: Toward a physically-based calving law, Geophysical Research Letters, 39, 2012.

Borstad, C., Rignot, E., Mouginot, J., and Schodlok, M.: Creep deformation and buttressing capacity of damaged ice shelves: theory and application to Larsen C ice shelf, The Cryosphere, 7, 2013.

Borstad, C., Khazendar, A., Scheuchl, B., Morlighem, M., Larour, E., and Rignot, E.: A constitutive framework for predicting weakening and reduced buttressing of ice shelves based on observations of the progressive deterioration of the remnant Larsen B Ice Shelf, Geophysical Research Letters, 2016.

Campbell, S., Roy, S., Kreutz, K., Arcone, S. A., Osterberg, E. C., and Koons, P.: Strain-rate estimates for crevasse formation at an alpine ice divide: Mount Hunter, Alaska, Annals of Glaciology, 54, 200–208, 2013.

Colgan, W., Rajaram, H., Abdalati, W., McCutchan, C., Mottram, R., Moussavi, M. S., and Grigsby, S.: Glacier crevasses: Observations, models, and mass balance implications, Reviews of Geophysics, 54, 119–161, 2016.

Cook, S., Rutt, I., Murray, T., Luckman, A., Zwinger, T., Selmes, N., Goldsack, A., and James, T.: Modelling environmental influences on calving at Helheim Glacier in eastern Greenland, The Cryosphere, 8, 827–841, 2014.

De Angelis, H. and Skvarca, P.: Glacier surge after ice shelf collapse, Science, 299, 1560–1562, 2003.

Delaney, A. and Arcone, S.: Crevasse detection with GPR across the Ross Ice Shelf, Antarctica, in: AGU Fall Meeting Abstracts, 2005.

Duddu, R. and Waisman, H.: A temperature dependent creep damage model for polycrystalline ice, Mechanics of Materials, 46, 23–41, 2012.

Duddu, R. and Waisman, H.: A nonlocal continuum damage mechanics approach to simulation of creep fracture in ice sheets, Computational Mechanics, pp. 1–14, 2013.

Dupont, T. and Alley, R.: Assessment of the importance of ice-shelf buttressing to ice-sheet flow, Geophysical Research Letters, 32, 2005.

Fretwell, P., Pritchard, H. D., Vaughan, D. G., Bamber, J., Barrand, N., Bell, R., Bianchi, C., Bingham, R., Blankenship, D., Casassa, G., et al.: Bedmap2: improved ice bed, surface and thickness datasets for Antarctica, The Cryosphere, 7, 2013.

Gagliardini, O., Zwinger, T., Gillet-Chaulet, F., Durand, G., Favier, L., De Fleurian, B., Greve, R., Malinen, M., Martín, C., Råback, P., et al.: Capabilities and performance of Elmer/Ice, a new-generation ice sheet model, Geoscientific Model Development, 6, 1299–1318, 2013.

Goldberg, D., Holland, D., and Schoof, C.: Grounding line movement and ice shelf buttressing in marine ice sheets, Journal of Geophysical Research: Earth Surface (2003–2012), 114, 2009.

Gudmundsson, G.: Ice-shelf buttressing and the stability of marine ice sheets, The Cryosphere, 7, 647–655, 2013.

Hosmer Jr, D. W. and Lemeshow, S.: Applied logistic regression, John Wiley & Sons, 2004.

Jacobs, S., Hellmer, H., Doake, C., Jenkins, A., and Frolich, R.: Melting of ice shelves and the mass balance of Antarctica, Journal of Glaciology, 38, 375–387, 1992.

Jansen, E., Overpeck, J., Briffa, K., Duplessy, J.-C., Joos, F., Masson-Delmotte, V., Olago, D., Otto-Bliesner, B., Peltier, W., Rahmstorf, S., Ramesh, R., Raynaud, D., Rind, D., O.Solomina, Villalba, R., and Zhang, D.: Palaeoclimate, in: Climate Change 2007: The Physical Science Basis, Contribution of Working Group I to the Fourth Assessment Report of the Intergovernmental Panel on Climate Change, Cambridge University Press, Cambridge, United Kingdom and New York, NY, USA, 2007.

Jezek, K. C.: A modified theory of bottom crevasses used as a means for measuring the buttressing effect of ice shelves on inland ice sheets, Journal of Geophysical Research: Solid Earth (1978–2012), 89, 1925–1931, 1984.

Johanson, C. M. and Fu, Q.: Antarctic atmospheric temperature trend patterns from satellite observations, Geophysical research letters, 34, 2007.

Kachanov, L.: Time of the rupture process under creep conditions, Izu, Akad. Nauk SSR Otd. Tech, pp. 26–31, 1958.

Katz, R. F. and Worster, M. G.: Stability of ice-sheet grounding lines, in: Proceedings of the Royal Society of London A: Mathematical, Physical and Engineering Sciences, p. rspa20090434, The Royal Society, 2010.

Kenneally, J. P. and Hughes, T. J.: Fracture and back stress along the Byrd Glacier flowband on the Ross Ice Shelf, Antarctic Science, 16, 345–354, 2004.

Khazendar, A., Rignot, E., and Larour, E.: Larsen B Ice Shelf rheology preceding its disintegration inferred by a control method, Geophysical Research Letters, 34, 2007.

Krug, J., Weiss, J., Gagliardini, O., and Durand, G.: Combining damage and fracture mechanics to model calving, The Cryosphere, 8, 2101–2117, 2014.

Larour, E., Rignot, E., Joughin, I., and Aubry, D.: Rheology of the Ronne Ice Shelf, Antarctica, inferred from satellite radar interferometry data using an inverse control method, Geophysical Research Letters, 32, 2005.

Larour, E., Seroussi, H., Morlighem, M., and Rignot, E.: Continental scale, high order, high spatial resolution, ice sheet modeling using the Ice Sheet System Model (ISSM), Journal of Geophysical Research: Earth Surface (2003–2012), 117, 2012.

Le Brocq, A. M., Payne, A. J., and Vieli, A.: An improved Antarctic dataset for high resolution numerical ice sheet models (ALBMAP v1)., Earth system science data., 2, 247–260, 2010.

Levermann, A., Albrecht, T., Winkelmann, R., Martin, M., Haseloff, M., and Joughin, I.: Kinematic first-order calving law implies potential for abrupt ice-shelf retreat, The Cryosphere, 6, 273–286, 2012.

Luckman, A., Jansen, D., Kulessa, B., King, E., Sammonds, P., and Benn, D.: Basal crevasses in Larsen C Ice Shelf and implications for their global abundance, The Cryosphere, 6, 113, 2012.

Mercer, J. H.: West Antarctic ice sheet and CO2 greenhouse effect: a threat of disaster, Ohio State University, Institute of Polar Studies, 1978.

Miles, B., Stokes, C., Vieli, A., and Cox, N.: Rapid, climate-driven changes in outlet glaciers on the Pacific coast of East Antarctica, Nature, 500, 563–566, 2013.

Morlighem, M., Seroussi, H., Larour, E., and Rignot, E.: Inversion of basal friction in Antarctica using exact and incomplete adjoints of a higher-order model, Journal of Geophysical Research: Earth Surface, 118, 1746–1753, 2013.

Morlighem, M., Bondzio, J., Seroussi, H., Rignot, E., Larour, E., Humbert, A., and Rebuffi, S.: Modeling of Store Gletscher's calving dynamics, West Greenland, in response to ocean thermal forcing, Geophysical Research Letters, 43, 2659–2666, 2016.

Motyka, R.: Deep-water calving at Le Conte Glacier, southeast Alaska, Byrd Polar Res. Cent. Rep, 15, 115–118, 1997.

Navarro, F. J., Macheret, Y. Y., and Benjumea, B.: Application of radar and seismic methods for the investigation of temperate glaciers, Journal of Applied Geophysics, 57, 193–211, 2005.

Nick, F., Van der Veen, C. J., Vieli, A., and Benn, D.: A physically based calving model applied to marine outlet glaciers and implications for the glacier dynamics, Journal of Glaciology, 56, 781–794, 2010.

Nick, F. M., Vieli, A., Andersen, M. L., Joughin, I., Payne, A., Edwards, T. L., Pattyn, F., and van de Wal, R. S.: Future sea-level rise from Greenland/'s main outlet glaciers in a warming climate, Nature, 497, 235–238, 2013.

Nye, J.: Comments on Dr Loewe's letter and notes on crevasses, Journal of Glaciology, 2, 512–514, 1955.

Otero, J., Navarro, F. J., Martin, C., Cuadrado, M. L., and Corcuera, M. I.: A three-dimensional calving model: numerical experiments on Johnsons Glacier, Livingston Island, Antarctica, Journal of Glaciology, 56, 200–214, 2010.

Pralong, A. and Funk, M.: Dynamic damage model of crevasse opening and application to glacier calving, Journal of Geophysical Research: Solid Earth, 110, 2005.

Pralong, A., Funk, M., and Lüthi, M. P.: A description of crevasse formation using continuum damage mechanics, Annals of Glaciology, 37, 77–82, 2003.

Price, S., Lipscomb, W., Hoffman, M., Hagdorn, M., Rutt, I., Payne, A., Hebeler, F., and Kennedy, J. H.: CISM 2.0. 0 Documentation, 2014.

Rignot, E., Mouginot, J., and Scheuchl, B.: Ice flow of the Antarctic ice sheet, Science, 333, 1427–1430, 2011a.

Rignot, E., Mouginot, J., and Scheuchl, B.: MEaSUREs InSAR-based Antarctica ice velocity map, Science, 333, 1427–1430, 2011b.

Shepherd, A., Ivins, E. R., Geruo, A., Barletta, V. R., Bentley, M. J., Bettadpur, S., Briggs, K. H., Bromwich, D. H., Forsberg, R., Galin, N., et al.: A reconciled estimate of ice-sheet mass balance, Science, 338, 1183–1189, 2012.

Smith, R.: The application of fracture mechanics to the problem of crevasse penetration, Journal of Glaciology, 17, 223–228, 1976.

Steig, E. J., Schneider, D. P., Rutherford, S. D., Mann, M. E., Comiso, J. C., and Shindell, D. T.: Warming of the Antarctic ice-sheet surface since the 1957 International Geophysical Year, Nature, 457, 459–462, 2009.

Van der Veen, C.: Fracture mechanics approach to penetration of surface crevasses on glaciers, Cold Regions Science and Technology, 27, 31–47, 1998a.

Van der Veen, C.: Fracture mechanics approach to penetration of bottom crevasses on glaciers, Cold Regions Science and Technology, 27, 213–223, 1998b.

Van der Veen, C.: Calving glaciers, Progress in Physical Geography, 26, 96–122, 2002.

Vaughan, D. G.: Relating the occurrence of crevasses to surface strain rates, Journal of Glaciology, 39, 255–266, 1993.

Vaughan, D. G., Marshall, G. J., Connolley, W. M., Parkinson, C., Mulvaney, R., Hodgson, D. A., King, J. C., Pudsey, C. J., and Turner, J.: Recent rapid regional climate warming on the Antarctic Peninsula, Climatic change, 60, 243–274, 2003.

Weertman, J.: Can a water-filled crevasse reach the bottom surface of a glacier, IASH Publ, 95, 139–145, 1973.